Journal of African Earth Sciences 112 (2015) 234–250

Contents lists available at ScienceDirect

Journal of African Earth Sciences

journal homepage: www.elsevier.com/locate/jafrearsci

Tephrostratigraphy and depositional environment of young (<2.94 Ma) Hadar Formation deposits at Ledi-Geraru, Afar, Ethiopia

Erin N. DiMaggio [a, *], J Ramón Arrowsmith [b], Christopher J. Campisano [c], Roy Johnson [d], Alan L. Deino [e], Mark Warren [f], Shimeles Fisseha [g], Andrew S. Cohen [d]

[a] Department of Geosciences, Pennsylvania State University, University Park, PA 16802, USA
[b] School of Earth and Space Exploration, Arizona State University, P.O. Box 871404, Tempe, AZ 85287, USA
[c] Institute of Human Origins, School of Human Evolution and Social Change, Arizona State University, P.O. Box 874101, Tempe, AZ 85287, USA
[d] Department of Geosciences, University of Arizona, 1040 E. 4th Street, Tucson, AZ 85721, USA
[e] Berkeley Geochronology Center, 2455 Ridge Road, Berkeley, CA 94709, USA
[f] ConocoPhillips, 600 N Dairy Ashford, Houston, TX 77079, USA
[g] Institute of Geophysics, Space Sciences and Astronomy, Addis Ababa University, P.O. Box 1176, Addis Ababa, Ethiopia

ARTICLE INFO

Article history:
Received 23 January 2015
Received in revised form
21 September 2015
Accepted 22 September 2015
Available online 30 September 2015

Keywords:
Afar depression
Hadar Formation
Pliocene
Tephrochronology
Stratigraphy
Hominin paleoenvironments

ABSTRACT

The Pliocene Hadar Formation, exposed throughout the lower Awash Valley, Ethiopia, chronicles the evolution and paleoenvironmental context of early hominins. Deposition of the Hadar Formation continued until at least 2.94 Ma, but what transpired in the Hadar Basin after this time remains poorly documented due to an erosional event that truncated the formation throughout much of the valley. Here we present geologic mapping and stratigraphic analysis of a 26 m-thick section of sedimentary rocks and tephras exposed in the Ledi-Geraru project area in the region of Gulfaytu. The section contains Hadar Formation strata younger than 2.94 Ma, and sediments that we interpret are Busidima Formation in age, <2.7 Ma. We use this record to place additional constraints on depositional environments and the tectonic and paleogeomorphic history of the region. The lower ~20 m of section contains lacustrine deposits that conformably overly a 2.94 Ma marker bed (BKT-2U) that previously served as the uppermost dated tephra in the Hadar Formation. We identified seven post-BKT-2U tephras; three were analyzed for glass chemistry, and one yielded an $^{40}Ar/^{39}Ar$ age of 2.931 ± 0.017 Ma (1σ). Based on these analyses, the newly mapped deposits at Gulfaytu extend the top of the Hadar Formation, representing ca. 20 kyr of post-BKT-2 sedimentation. The Hadar Basin remained depositional following the BKT-2 eruptions, and paleolake Hadar was present at Gulfaytu at this time. An erosional surface marked by a conglomerate truncates the Hadar strata suggesting that the Gulfaytu region was also was influenced by significant changes to basin architecture well-documented elsewhere in the lower Awash Valley. In addition, geophysical models suggest that central Ledi Geraru hosts a thick subsurface lacustrine sedimentary record within the Hadar Basin. The results of this paper provide the outcrop and near surface characterization for the Hominin Sites and Paleolakes Drilling Project (HSPDP) effort at Gulfaytu.

1. Introduction

Plio-Pleistocene sedimentary sequences in the Afar Depression, Ethiopia archive sedimentary records of continental breakup and host fossil and stone tool assemblages that chronicle hominin evolution and innovation. Active volcanism, tectonic-driven basin subsidence, and Late Cenozoic climate change drove patterns of sedimentation and drainage reorganization, building complex sedimentary records (Fig. 1; Campisano and Feibel, 2007; deMenocal, 1995, 2004; Hayward and Ebinger, 1996; Trauth et al., 2007). The resulting deposits contain high concentrations of volcanic material including datable tephra layers (WoldeGabriel et al., 2000) and an extensive collection of mammalian fossils including hominins (e.g., Alemseged et al., 2006; Haile-Selassie et al., 2010; Johanson et al., 1982; Kimbel, 1996; Kimbel et al., 1994; Semaw et al., 2005; White et al., 2009, 2003; 2006) enabling the construction of temporally constrained stratigraphic records that document the progression of paleolandscapes in which early

* Corresponding author.
E-mail address: dimaggio@psu.edu (E.N. DiMaggio).

http://dx.doi.org/10.1016/j.jafrearsci.2015.09.018
1464-343X/

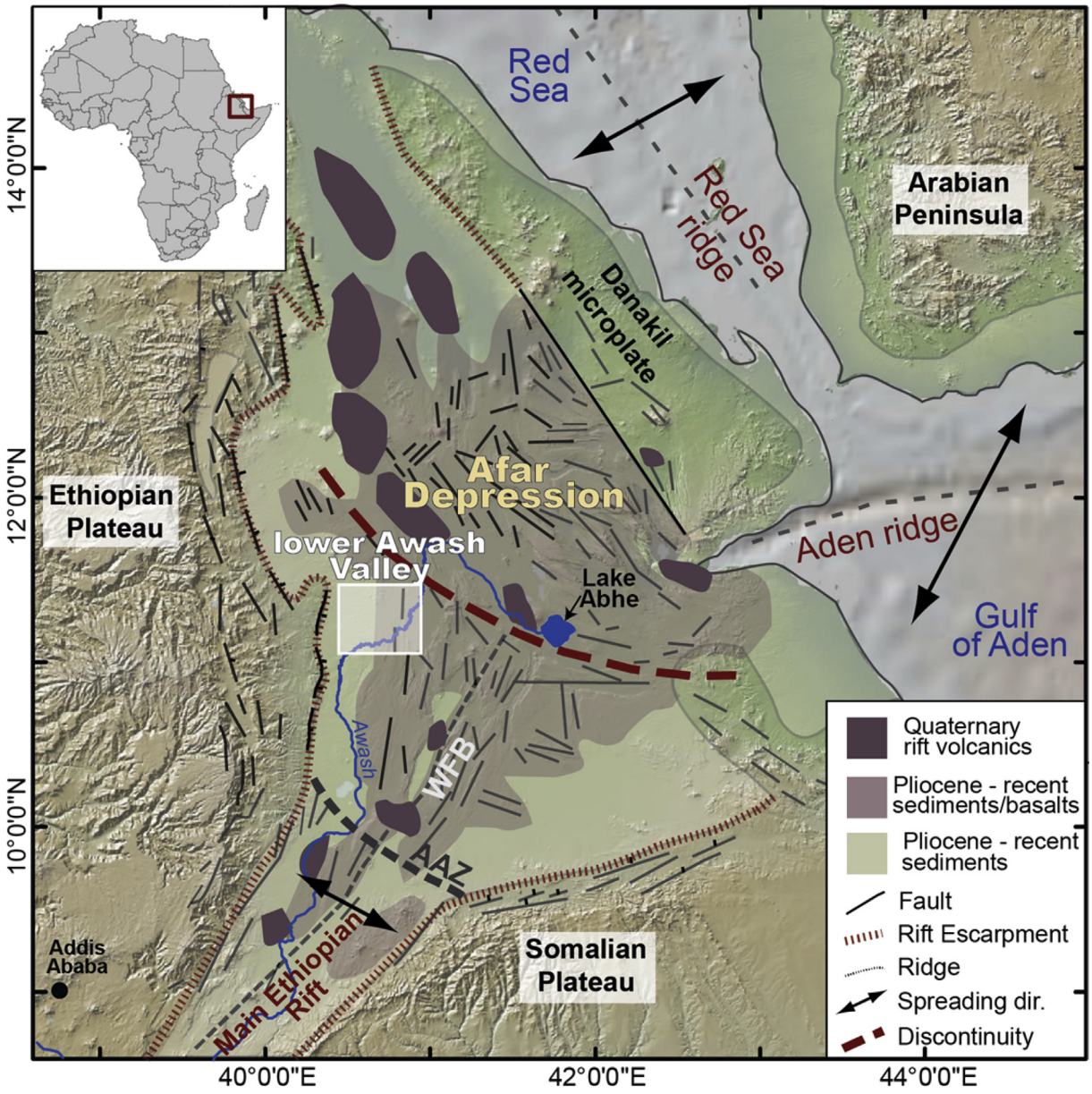

Fig. 1. Overview map of the Afar Depression, Ethiopia, showing major structural trends and extension directions (black arrows), topographic features, and the distribution of volcanic rocks and sediments. The lower Awash Valley lies south of a discontinuity that marks the northern extent of extension along the Main Ethiopian Rift. AAZ denotes the arcuate accommodation zone (Tesfaye et al., 2003), WFB = Wonji fault belt, and a white box outlines extent of the lower Awash Valley (Fig. 2).

hominins lived.

In the lower Awash Valley, late Quaternary river incision has exposed thick sedimentary sequences in Miocene to Pleistocene aged rift basins, including the Pliocene Hadar Formation. Deposited in the Hadar Basin, the Hadar Formation is widely recognized for its exceptionally rich collection of fossil fauna within gently dipping fluvio-lacustrine deposits. Basin models have been developed to explain the sedimentation history of the Hadar Formation (Quade et al., 2008; Tiercelin et al., 1986; Wynn et al., 2008), however we lack constraints on the extent of the Hadar Basin and the location and length of border faults that controlled its subsidence history. Sometime between 2.9 and 2.7 Ma, the sedimentary system changed in the lower Awash region as it responded to the formation of the Busidima sedimentary basin and deposition of predominately fluvial sediments of the Busidima Formation (Quade et al., 2004, 2008; Wynn et al., 2008). The timing and nature of this transition, including details of environmental and biological change, remains unclear because sediments spanning this time period (2.9–2.7 Ma) were mostly eroded in the Hadar area and an unconformity now marks this event in the regional stratigraphy. Finding and describing sedimentary rocks that are 2.9–2.7 Ma in other areas of the lower Awash provide important controls on tectonosedimentary basin models and reconstructing paleoenvironments of early *Homo* (DiMaggio et al., 2015; Villmoare et al., 2015).

In this contribution, we report on the geology of Gulfaytu, a region in the Ledi-Geraru Research Project (LGRP) area in the lower Awash Valley (Figs. 1 and 2). We present a geologic map, stratigraphic sections, and the chemistry and radiometric age of tephra deposits that document Hadar Formation strata overlying a 2.94 Ma

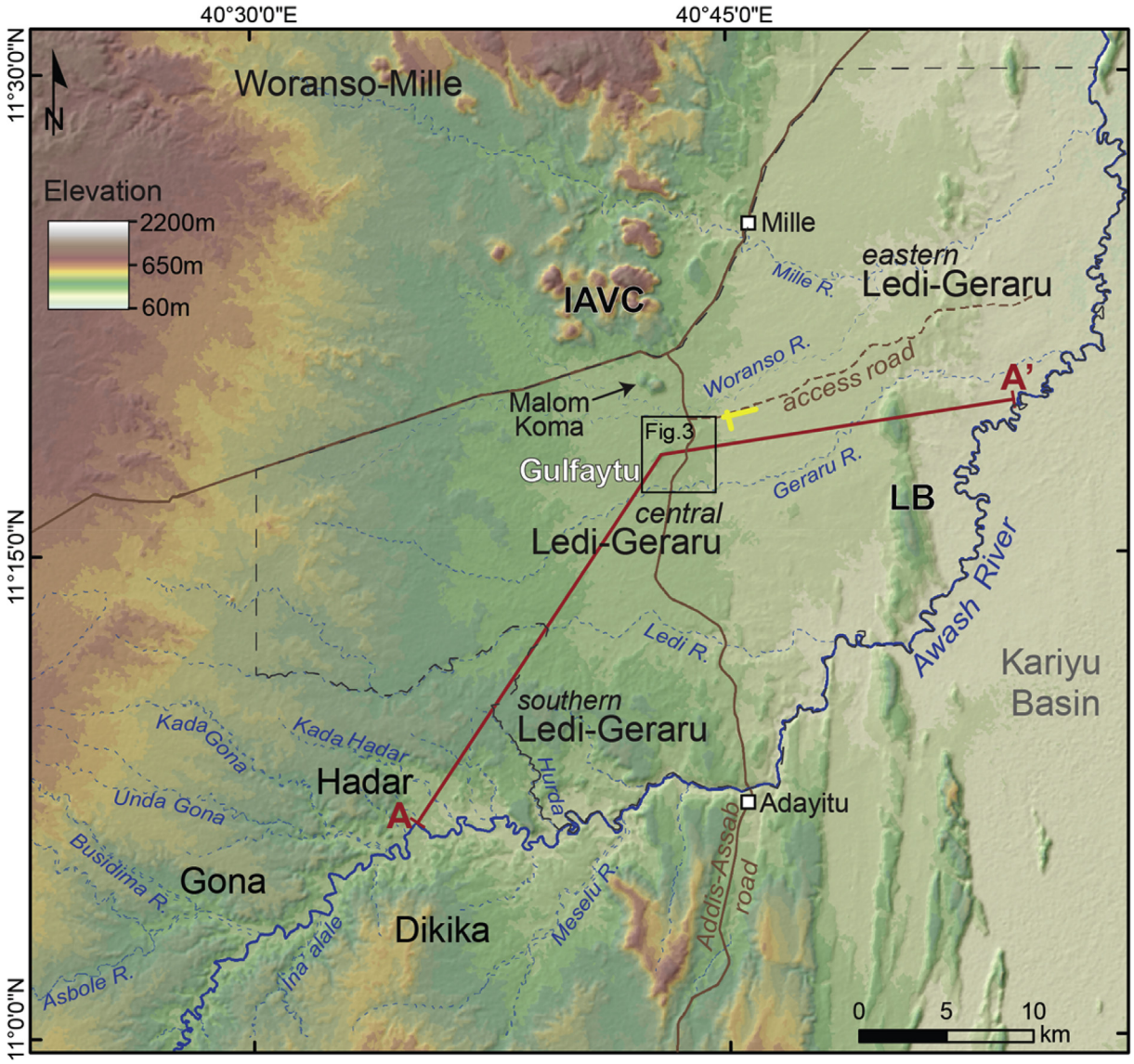

Fig. 2. Shaded relief map of the lower Awash Valley showing project areas and geographic features. The Pliocene Hadar Basin encompasses much of this area, though its boundaries are not well-constrained. A black rectangle outlines the area mapped at Gulfaytu in Fig. 3, and the dashed black line denotes the Ledi-Geraru project area. Yellow lines mark the location of seismic surveys shown in Fig. 8 and a red line (A to A') denotes the cross section line interpreted in Fig. 9. IAVC – Ida Ale Volcanic Complex; LB – Laa Yaggili basalt ridge. (For interpretation of the references to colour in this figure legend, the reader is referred to the web version of this article.)

marker bed tephra (BKT-2U), and Busidima Formation-age strata. These investigations, combined with reflection seismic observations of the subsurface, increase the known spatial and temporal extent of the hominin-bearing Hadar Formation and provide a new suite of tephra deposits for possible correlations to un-assigned sedimentary packages elsewhere in the region. We summarize our observations with a cross-section that offers insights into the sedimentary and structural development of the lower Awash Valley, and provides the geological framework and justification for the placement of the northern Awash Hominin Sites and Paleolakes Drilling Project (HSPDP) scientific drilling sites (Cohen et al., 2009; Cohen and Umer, 2009; Gibbons, 2013).

2. Geologic context

The structural and volcanic development of Afar, Ethiopia, is controlled by the complex intersection of continental (Main Ethiopian rift -MER) and oceanic rifting (Red Sea and Gulf of Aden spreading centers) (Fig. 1). The Afar triple junction, formed by the intersection of these rift segments, was first established when NNW-SSE directed extension propagating northward along the MER reached the southern Afar ca. 11 Ma (Wolfenden et al., 2004). Since then, the triple junction has continued propagating northeast, overprinting older structures, to its current position in the vicinity of Lake Abhe (Tesfaye et al., 2003). Sedimentary basin architecture in the Afar is modified by the interplay of these structures, which have influenced the spatial and temporal pattern of depositional environments. The LGRP area in the lower Awash Valley is situated in the southern tectonic province of the Afar Depression, south of the Tendaho discontinuity separating NE-SW directed extension in central Afar from predominately NNW-SSE extension in southern Afar (Fig. 1). Ledi-Geraru is located along the base of the Ethiopian escarpment within a series of marginal lowland basins (<1 km elevation). The active central grabens of the MER, part of the Wonji Fault Belt, lie ~50 km southeast of Ledi-Geraru (Fig. 1).

The Pliocene-Pleistocene volcanic rock record in the Afar is dominated by the expansive Afar Stratoid Series flood basalts (~3.5–1 Ma; Barberi et al., 1975; Kidane et al., 2003; Lahitte et al., 2003) and the Dahla Series flows (~4–8 Ma; Audin et al., 2004; Barberi et al., 1975). The Stratoid Series flows interfinger with the Pliocene Hadar Formation and form prominent fault bounded ridges throughout the lower Awash Valley that contrast with the sediment record.

2.1. Chronostratigraphy

Decades of focused geological and paleontological research in the lower Awash Valley, largely associated with understanding the stratigraphic and paleoenvironmental context for vertebrate fossils, has resulted in a robust chronostratigraphic sequence for the Hadar and Busidima Formations, part of the Awash Group strata. The Hadar Formation (ca. 3.80–2.94 Ma) is a thick (up to 230 m), relatively flat lying sequence of fluvial, lake-margin, and lacustrine sediments that yields over 90% of the known fossil remains of *Australopithecus afarensis*, including "Lucy" and "Selam" (Alemseged et al., 2006; Campisano and Feibel, 2008a; Johanson and Taieb, 1976; Kimbel and Delezene, 2009; Taieb et al., 1976; Wynn et al., 2006). Based on the stratigraphic nomenclature of Taieb et al. (1976), the Hadar Formation is divided into four members, temporally calibrated by paleomagnetic records and $^{40}Ar/^{39}Ar$ dating of tephra beds. These members include the Basal (~3.80–3.42 Ma), Sidi Hakoma (~3.42–3.24 Ma) Denen Dora (~3.24–3.20 Ma), and Kada Hadar (~3.20–2.94 Ma) (Semaw et al., 1997; Walter, 1994; Walter and Aronson, 1993; Wynn et al., 2008). The lower boundary of the Hadar Formation was recently defined as the contact between 8 and 4 Ma Dahla Series basalt flows and >3.8 Ma Basal Member sediments (Wynn et al., 2008). A widespread angular unconformity surface termed the Busidima unconformity surface (BUS; Quade et al., 2004; Wynn et al., 2008) defines the top of the Hadar Formation and separates the Hadar Formation from the overlying Busidima Formation. The Bouroukie Tuff 2 (BKT-2) complex (referring to three tephras: Green Marker Bed (GMB), BKT-2L, and BKT-2U; Campisano and Feibel, 2008a; Walter, 1981) lies in the youngest Kadar Hadar Member strata. BKT-2L and BKT-2U are dated to 2.96 and 2.94 Ma, respectively (Campisano, 2007; DiMaggio et al., 2008; Semaw et al., 1997) and provide the previous upper age estimate for the Hadar Formation. The BUS truncates the Hadar Formation to different stratigraphic levels, leaving only sparse outcrops of post-BKT-2 Kada Hadar Member sediments across the lower Awash. Prior to this study, the thickest known post-BKT-2 Kada Hadar Member strata are at the Hadar project site (Fig. 2), but they are less than 8 m thick, laterally discontinuous, and do not contain tephras (Campisano and Feibel, 2008a). In contrast to the Hadar Formation, the Busidima Formation (2.69–0.16 Ma) contains high-energy fluvial cut and fill sequences that contain many erosional unconformities. Busidima sediments have been mapped throughout Gona (~130 m thick; Quade et al., 2004; Quade et al., 2008), Dikika (~145 m thick; Wynn et al., 2008), and Hadar (~40 m thick; Campisano, 2012) and have yielded fossil hominins (*Homo* aff., *H. habilis* and *Homo erectus*) and stone tools (Kimbel et al., 1996; Quade et al., 2004; Semaw et al., 2003; Simpson et al., 2008).

2.2. Basin framework

Syntheses of the lower Awash stratigraphic record offer insights into the structural controls that modulated the spatial and temporal depositional patterns observed in the Hadar and Busidima Formations. The basin models of Tiercelin et al. (1986) and Quade et al. (2008) showed that during the deposition of the Hadar Formation (3.80–2.94 Ma) the primary extension direction followed that of the MER (approximately east-west extension; Fig. 1). Wynn et al. (2008) argued that the Hadar Basin extended to the northeast-southwest, following the opening direction of the Red Sea rift (Fig. 1). For both models, the Hadar Basin depocenter was located northeast of the Hadar and Dikika project sites (Fig. 2). By ~2.7 Ma, changes in regional tectonics led to a reconfiguration of basin architecture in the lower Awash. Activity along the N–S trending As Duma border fault in western Gona (Quade et al., 2004) created the Busidima half-graben in an area that was once part of the Hadar Basin, and accommodation space for the deposition of the Busidima Formation. Changes in basin architecture, along with changes in climate (deMenocal, 1995), influenced depositional environments (e.g., Wynn et al., 2008), ecosystems, and faunal communities (e.g., Reed, 2008), but the intervening time period (2.9–2.7 Ma) has remained undocumented in the lower Awash until recently (DiMaggio, 2013; DiMaggio et al., 2015). Additionally, resolving the location and length of the Hadar Basin border faults and mapping the eastern flexural margin of the Busidima half-graben remain outstanding problems for understanding the regional structural development of the Afar Depression.

2.3. Previous work in the Ledi-Geraru project area

Ledi-Geraru is located adjacent to the Hadar, Dikika, and Woranso-Mille project areas (Fig. 2). Investigations of the southern Ledi-Geraru strata extending north from the Awash River have shown that the Hadar Formation is > 250 m thick, exposing the Sidi Hakoma and Denen Dora Members, and isolated outcrops of the Kada Hadar Member (Fig. 2; Arrowsmith et al., 2004; Dupont-Nivet et al., 2008). Whereas coeval fluvio-lacustrine sediments at Hadar and Gona (west of Ledi-Geraru) are marked by comparatively slow sedimentation (~30 cm/kyr; Campisano and Feibel, 2007), sedimentation rates measured in southern Ledi-Geraru are consistently high (~90 cm/kyr; Dupont-Nivet et al., 2008) reflecting dominantly lacustrine deposition in a continuously subsiding basin. Outcrops of BKT-2U are mapped across southern and central Ledi-Geraru indicating the northeastern continuation of the Hadar Formation (DiMaggio et al., 2008). Recent work documenting the geology of eastern Ledi-Geraru (DiMaggio, 2013; DiMaggio et al., 2015) has confirmed the presence ca. 2.8 Ma sedimentary deposits, however their stratigraphic relationship to the Hadar or Busidima Formation is not yet clear.

This study focuses on the Gulfaytu region of central Ledi-Geraru located between the Woranso and Geraru drainages along the Addis-Assab road (Figs. 2 and 3). Geologic data from surrounding project areas strongly support the central Ledi-Geraru, including Gulfaytu, as a Pliocene lacustrine depocenter at least during the deposition of the Hadar Formation (~3.8–2.94 Ma). Evidence for this assertion includes the high deposition rates of the Hadar Formation at Ledi-Geraru with north and eastward thickening and dip (Campisano and Feibel, 2008a; Dupont-Nivet et al., 2008; Quade et al., 2008; Taieb et al., 1976; Wynn et al., 2008), a northeastern increase in lacustrine dominated sediments, including diatomite facies encasing BKT-2U at Ledi-Geraru (DiMaggio et al., 2008), and a north/northeast-directed paleotributary system at Hadar (Behrensmeyer, 2008).

3. Methodology

3.1. Geologic mapping and stratigraphy

We mapped the geology of a 4 × 4 km region in Gulfaytu at a scale of 1:6000 using anaglyphs created from 1994 stereo aerial photographs from the Ethiopian Mapping Agency and WorldView-

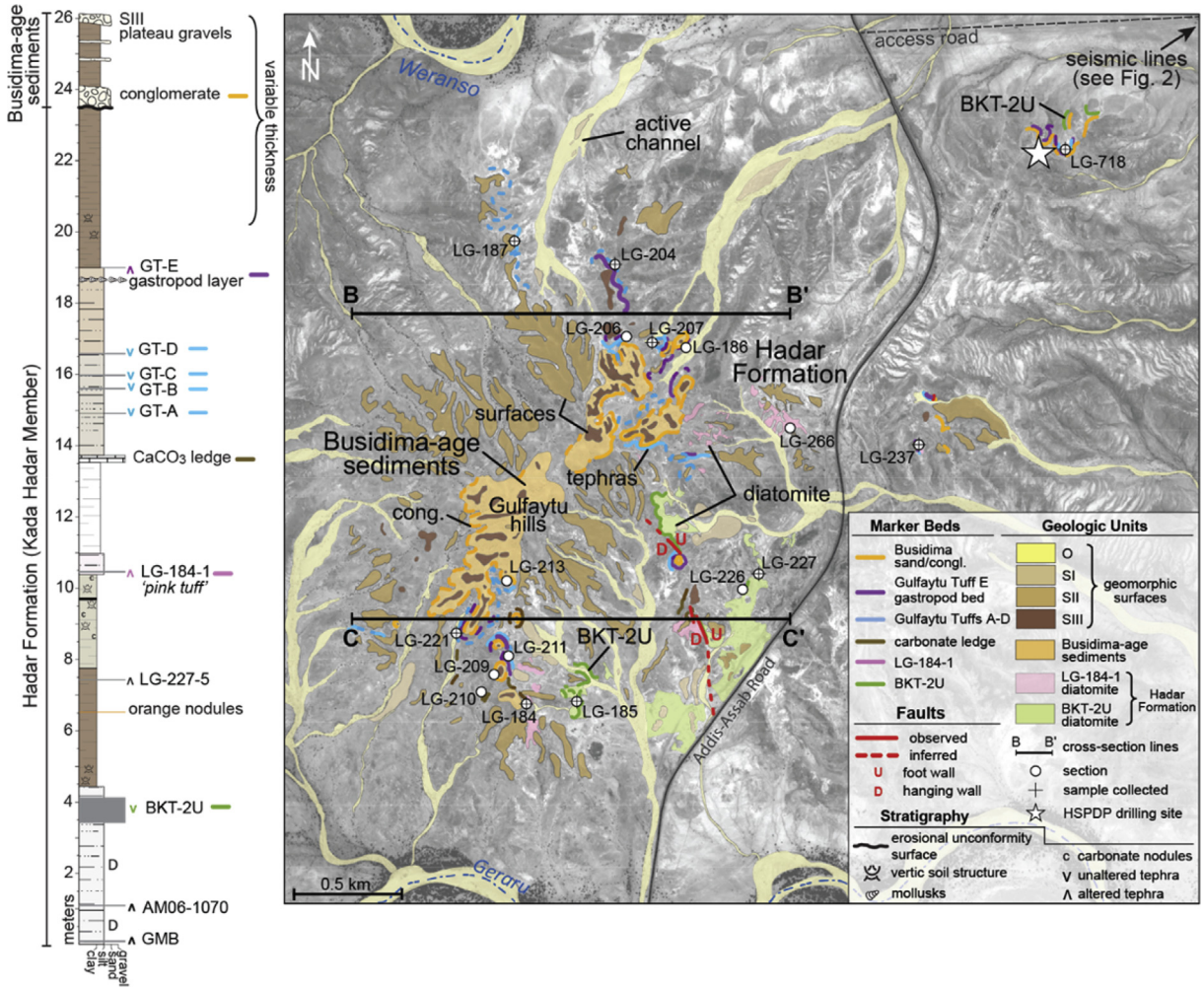

Fig. 3. (left) Composite stratigraphic section of the Hadar Formation and Busidima-age sediments mapped at Gulfaytu in the central Ledi-Geraru project area. Note the presence of BKT-2U near the base of the section. (right) Geologic map overlaying high resolution imagery where sediments including and overlying BKT-2 are exposed within ~26 m of relief. We mapped the Gulfaytu Tuffs (A through D) as a singular unit due to their close stratigraphic position, but in many cases all four tephras were not exposed in a singular outcrop. The seismic lines shown in Fig. 2 (yellow lines) are located ~1.5 m northeast of the HSPDP drilling site denoted by a star. Fig. 2 shows the extent of the geologic map, and cross section lines B-B' and C-C' are interpreted in Fig. 4.

2 satellite imagery (0.5 m resolution) as base maps in the field. Stratigraphic sections were measured at multiple locations throughout Gulfaytu and described at decimeter-scale (Figs. 3 and 4). The stratigraphic context of Gulfaytu tephras guided our sampling strategy (Figs. 5 and 6); we sampled tephras when they could not be traced across the landscape or when a new tephra was observed in section.

3.2. Glass chemistry

The chemistry of ten tephra samples were analyzed using an electron microprobe (EMP) and compared with published analyses of tephras from the Hadar Formation (~3.8–2.94 Ma) and lower Busidima Formation (~2.7–2.2 Ma) at the Hadar, Dikika, Gona, and Ledi-Geraru project areas. Statistical distance (SD) analysis (n = 6 elements) was initially used to determine possible correlates based on glass chemistry (Perkins et al., 1995). In addition to glass chemistry, we compared stratigraphic positions, physical descriptions, bed thicknesses, and clast morphology, all of which contributed to determining tephra correlations.

Tephra samples were prepared and analyzed following established methods used by other lower Awash valley researchers (e.g., Roman et al., 2008). To prepare tephra for geochemical analysis, we immersed tephra samples in water overnight, which reduced the need for mechanical crushing. Samples were wet-sieved to remove fine particles (<0.125 μm), and depending on the coarseness of the sample, we retained either the >250 μm or >420 μm size fractions. When necessary, a Frantz isodynamic magnetic separator was used to isolate the non-magnetic vitric component. A portion of each sample was agitated in a 5% HF ultrasonic bath for 1–2 min to remove adhering clays, and rinsed 3–4 times in distilled water. All remaining clay fragments or other impurities were hand-picked to obtain a pure vitric split. Samples were mounted in 1-inch round epoxy thick sections, polished using a 0.25 μm diamond powder, and carbon coated (~150 ± 25 Å carbon film; Kerrick et al., 1973). We measured the major element chemistry of glass shards using wavelength-dispersive (WD) spectrometry on a JEOL JXA-8600 Superprobe (2006 and 2010 analyses) or a JEOL JXA 8530F Hyperprobe (2013 and 2015 analyses) at Arizona State University. We analyzed multiple tephra samples on both machines to insure results were consistent and reproducible. Both instruments were run at 15 kV, with a 10 nA beam current, and a defocused the beam (15 μm) to minimize alkali loss (Froggatt, 1992; Hunt and Hill, 1993). All data were corrected using atomic number (Z),

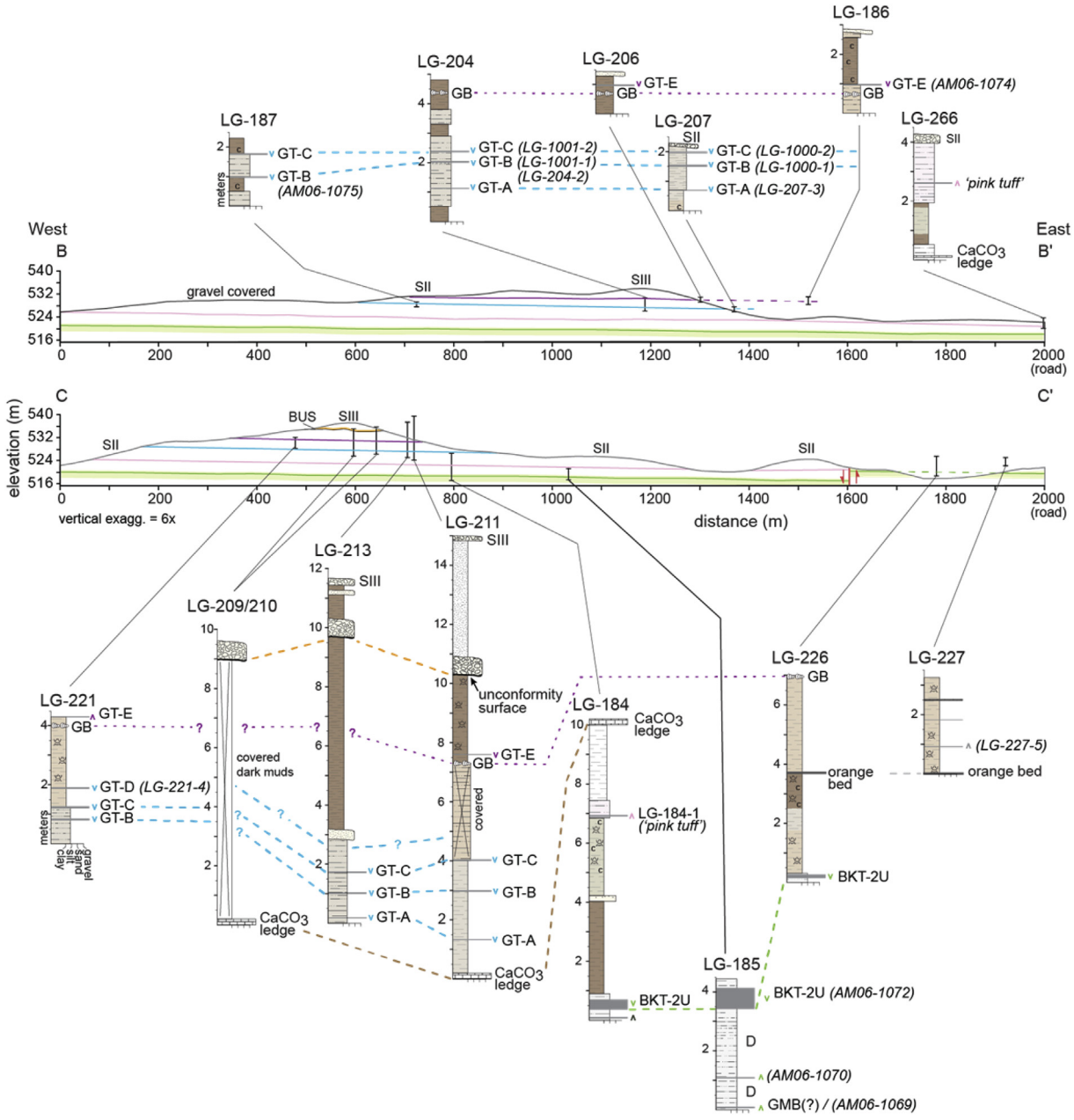

Fig. 4. Stratigraphic sections of the Hadar Formation and Busidima-age sediments at Gulfaytu projected and shown on cross section lines B and C, (section line locations are shown on Fig. 3). The number above each section (LG-xxx) refers to the locality ID shown in Fig. 3, and the gastropod bed is labeled as GB. Tephras collected are denoted with a sample ID number (LG-xxx-x or AM06-xxx) and those correlated across the field area are linked with a dashed line.

absorption (A), and fluorescence (F) corrections. Analytical conditions, including peak and background times and standards used for calibration, are presented in Table A.1.

3.3. $^{40}Ar/^{39}Ar$ dating

Careful inspection of each tephra horizon at Gulfaytu above BKT-2 revealed one devitrified tuff (sample LG-184-1) ~5–6 m stratigraphically above BKT-2U that contained feldspar phenocrysts suitable for dating. Crystals from LG-184-1 were prepared following standard procedures as outlined by Deino et al. (2010). The sample was wet sieved and the >250 μm size fraction retained. Feldspar grains were isolated using a Frantz isodynamic magnetic separator, and heavy liquids (LST) were used to separate sanidine from plagioclase. Inclusion-free grains were hand-selected under a microscope, treated with a 5% HF solution for 2–3 min in an ultrasonic bath, and rinsed 4 times in distilled water.

The feldspar crystal concentrate from sample LG184-1 was irradiated for four hours in the Cd-lined, in-core CLICIT facility of the Oregon State University TRIGA reactor. Sanidine from the Alder Creek Rhyolite was used as a mineral standard to evaluate neutron fluence, with a reference age of 1.202 Ma (Renne et al., 1998 adjusted for Kuiper et al., 2008). Standards and unknowns were placed in 2 mm diameter by 2 mm deep wells situated in a ring configuration of 16 holes near the edge of a 16.5 mm diameter, 2.5 mm thick aluminum disk (Best et al., 1995). Standards were spaced every five holes (i.e., four standard positions at 90° separation). Sanidine standards were analyzed by a five-step

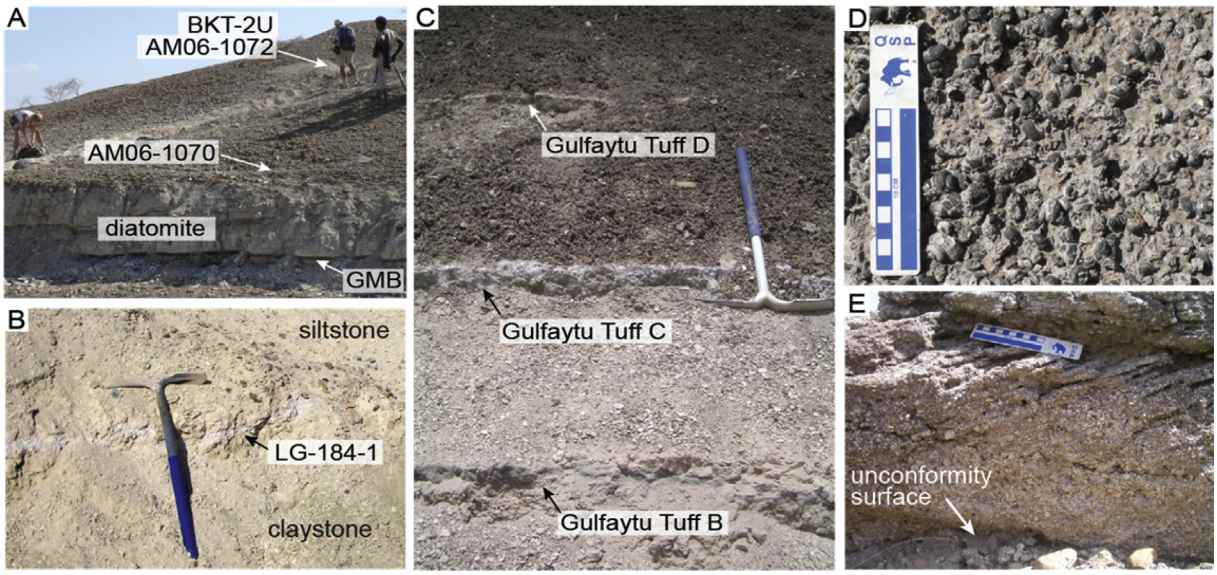

Fig. 5. Photographs from Gulfaytu. (A) BKT-2 encased in diatomite exposed along a wash at site LG-185. (B) Tan silts encasing a light pink bentonite layer containing feldspar crystals (sample LG-184-1). (C) Outcrop expression of Gulfaytu Tuffs B, C, and D at site LG-221. (D) 2–5 cm thick gastropod (*Bellamya*) bed consistently identified 20 cm below Gulfaytu Tuff E (LG-186). (E) An unconformity surface and the planar cross bedded carbonate-rich pebble conglomerate at LG-213 marking the base of Busidima-age sediments at Gulfaytu. (For interpretation of the references to colour in this figure legend, the reader is referred to the web version of this article.)

incremental heating experiment on single grains 500–600 microns in size in a manner similar to unknowns, as described below. The neutron fluence parameter, *J*, was calculated based on the weighted mean of the integrated gas composition of six incremental heating experiments for each irradiation position. Integrated gas compositions were used instead of plateau ages because the former more closely replicate the single-grain total-fusion sanidine experiments reported in Renne et al. (1998). Planar regressions were fit to the standard data, and *J* was interpolated for the unknowns. Residuals calculated for the standard positions from these regressions are typically less than ±0.2%, and Monte Carlo simulations of predicted *J* uncertainties are typically less than ±0.3%.

$^{40}Ar/^{39}Ar$ extractions were performed using a rampable 50 Watt CO_2 laser, fitted with a circular integrator lens, to incrementally heat individual feldspar crystals and liberate trapped argon. Single feldspar grains ~0.5–1 mm in size were heated for 30 s using a 2.3 mm diameter beam at power levels ranging from 0.8 to 7 Watts in 5–7 steps. Evolved gasses were exposed for several minutes to an approximately −130 °C cryosurface to trap H_20, and a GP-50 SAES getters to remove reactive compounds (CO, CO_2, N_2, O_2, and H_2).

Argon isotopic measurements were performed on a *Noblesse* 5-collector sector-magnet mass spectrometer, configured with one axial Faraday detector and four off-axis, symmetrically arrayed ETP ion counters. Prior to inlet of sample gas from the extraction line for determination of argon isotopic composition, a 3% aliquot of the extraction line volume was measured on the mass spectrometer within a short (~7 s) interval. On the basis of this 'sniff,' adjustments were made, if necessary, to the sample gas abundance in the extraction line by pumping away a calibrated fraction of the gas to evacuated ballast volumes. The goal of this procedure was to restrict the signal level of ^{40}Ar on the ion counters to less than 250 kcps across all experiments on this machine, corresponding to a maximum ^{40}Ar of ~3×10^{-15} mol. Typically, volume splitting was unnecessary, given the age, size, and potassium content of the feldspars, accompanied by careful adjustment of the step-heating schedule, such that signal levels were typically 150 kcps or below. Subsequent to this test protocol, the remainder of the sample gas was inlet to the mass spectrometer and five argon isotopes measured over a period of ~600 s. The isotopic measurement process involved simultaneous measurement of ^{40}Ar, ^{37}Ar, and ^{36}Ar on separate ion counters, alternating with peak hopping to position ^{38}Ar and ^{39}Ar on the same ion counter as ^{40}Ar.

All signals were normalized to the ^{40}Ar ion counter. ^{36}Ar signal normalization was achieved through periodic measurement of the $^{40}Ar/^{36}Ar$ ratio of air argon (298.6; Lee et al., 2006) inlet alternately from two separate standard gas reservoir and pipetting systems (one spiked with ^{39}Ar, the other pure air). Air abundances from these experiments were closely matched to the unknowns, yielding 2.5×10^{-15} and 2.3×10^{-15} mol ^{40}Ar from the spiked and unspiked systems, respectively. ^{37}Ar and ^{38}Ar signal normalizations were achieved through periodic measurement of ^{40}Ar from a static gas sample on relevant detectors in a systematic round-robin peak-hopping procedure. Procedural blanks, matching sample gas extractions precisely but without firing the laser, were run every 2–3 analyses and typically yielded ~6×10^{-17}, 4×10^{-19}, and 4×10^{-19} mol of ^{40}Ar, ^{39}Ar, and ^{36}Ar, respectively.

3.4. Seismic reflection data acquisition and processing

At Ledi-Geraru, areas of low topographic relief along access roads provide good conditions for geophysical profiling of the subsurface. In 2008, we conducted a seismic reflection survey in the flat expanses of central Ledi-Geraru, approximately parallel to the Woranso drainage and ~2 km east of the main Addis-Assab Road and the northernmost BKT-2 exposures (Fig. 2) to assess the depths of the sedimentary fill and basalt flows and to detect any buried volcanic ridges. Two roughly perpendicular reflection profiles were acquired; the main N 77° E profile (Line 1) was ~2.0 km long, and a S 14° E cross-line profile (Line 2) was ~1.1 km long. Seismic data collection was done using a 45-kg nitrogen-gas-charged accelerated-weight-drop (AWD) seismic source mounted on the back of a Toyota Land Cruiser. Seismic impulses were recorded using only the vertical components on Sercel L-28-3D 4.5-Hz three-component geophones. Single geophones were used at each recording station. These geophones were used because they provided a relatively broad frequency range (including low frequencies) and high

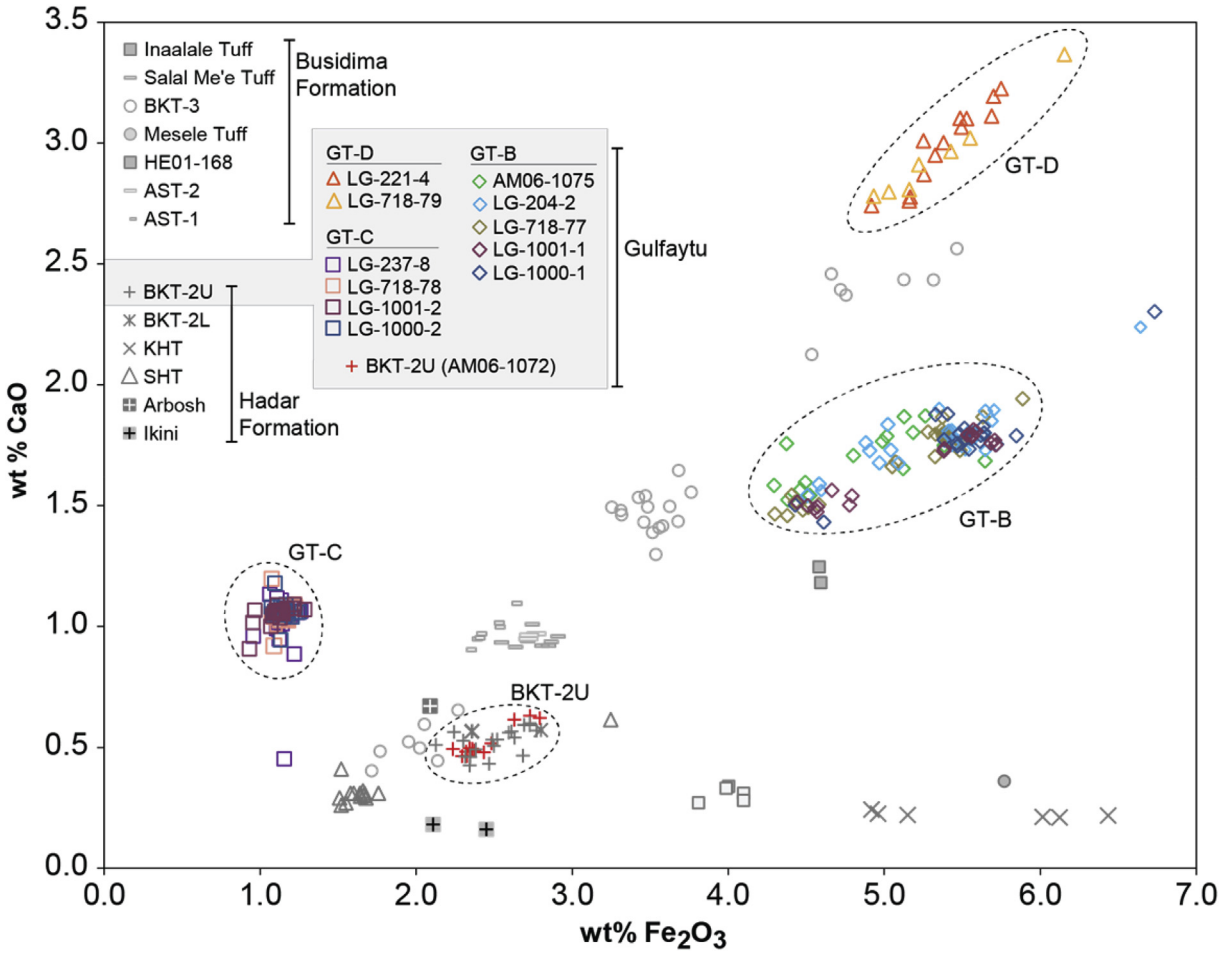

Fig. 6. Bivariate plot (CaO versus Fe_2O_3) of normalized glass shard analyses for tephras collected at Gulfaytu (individual analyses are shown for each sample in color), compared with average compositions of Hadar and select (<~2 mya) Busidima tuffs (grayscale; Campisano and Feibel, 2008b; DiMaggio et al., 2008; Dupont-Nivet et al., 2008; Quade et al., 2008; Wynn et al., 2006; Wynn et al., 2008). Only the high silica mode is shown; the composition of basaltic glass shards are provided in Table A.2. See Appendix A for analytical running conditions (Table A.1.) and major element chemistry for individual glass shards (Table A.2.). (For interpretation of the references to colour in this figure legend, the reader is referred to the web version of this article.)

sensitivity; signals generated by weight-drop sources used on loosely consolidated lake-bed sediments tend to be low frequency, and higher frequencies attenuate rapidly. To enhance signal fidelity and decrease environmental noise, each geophone was buried up to ~10 cm below the ground surface. Geophone responses were normally recorded using 3 24-channel Geode data loggers (72 active channels). At the end of Line 2 (where no additional equipment moves were necessary), 88 geophones were recorded into 4 24-channel Geode data loggers (88 active channels). Geophones were spaced every 5 m along each profile and source impacts were recorded at every other station (10-m spacing).

Data quality for each shot record varied depending on location and surface conditions of the source and the receivers, but was improved by summing 10 source impacts at each source point. Overall data quality was mixed, with clear reflections visible in many shot records and refractions related to shallow interfaces also evident. Surface waves ("ground-roll"), which are an inherent problem for all near-surface recording using weight-drop sources, were quite strong. This energy tended to have low velocities and interfered with data quality at greater offsets with increasing recording time. These noise sources were removed as much as possible ("muted" and filtered) during data processing.

Data processing was performed at the University of Arizona using standard data processing procedures (Yilmaz, 2001). Tomographic inversion of refraction arrivals provided tomographic velocity estimates to depths of ~150 m that were used as guides for normal-moveout (NMO) corrections. Below these depths, velocities were determined by constant-velocity-stack (CVS) analysis. Final stacking velocities were smoothed across the surveys to minimize high-frequency velocity changes due to picking errors or spurious noise. Normally, 18 common-midpoint (CMP) field traces were stacked for each final seismic trace to produce 18-fold data. Data quality of the processed profiles is fairly good to 0.2–0.3 s two-way travel time (approximate depths of ~150–300 m), but signal penetration decreased significantly below these depths.

4. Results

4.1. Gulfaytu geology

Gulfaytu exposes a ~26 m thick sequence of gently-dipping lacustrine and fluvial deposits that contain numerous tephra beds capped by late Quaternary gravel surfaces (also referred to as plateau gravels) along a broad NE-SW trending ridgeline informally referred to as the Gulfaytu hills (Figs. 3 and 4). The stratigraphy of this new extension of the Hadar Formation and descriptions of Busidima-age sediments are presented below.

4.1.1. Hadar Formation at Gulfaytu

We mapped BKT-2U (the uppermost of the BKT-2 deposits) along the low relief drainages at Gulfaytu, serving as a marker bed that denotes the base of the 26 m thick stratigraphic section (Fig. 3). At project areas adjacent to Ledi-Geraru, BKT-2 deposits are described as encased in brown mudstones (e.g., Campisano and Feibel, 2008a; Walter, 1981). However, at Gulfaytu BKT-2U is observed in a >4 m thick massive to fissile white silty diatomite (Fig. 5A), similar to descriptions from other localities east of Gulfaytu (DiMaggio et al., 2008). With no evidence of a depositional hiatus, BKT-2U and encasing diatomite are overlain by a 3–4 m thick dark to medium brown pedogenically modified mudstone that in some localities (e.g., LG-226) contains a thin tephra (sample LG-227-5). The overlying ~3 m, is a tan to light pink-colored diatomaceous silt that preserves a thin altered tephra (bentonite) layer at some locations (sample LG-184-1). An undulating 10 cm thick $CaCO_3$ layer caps the siltstone (Fig. 5B). In the ~6 m above the carbonate layer, tephras referred to as Gulfaytu Tuff A (GT-A) through Gulfaytu Tuff E (GT-E) are observed (Fig. 4). The tephras are encased in light brown silty clays (below GT-B) or darker mudstones (above GT-C) that show minor pedogenic alteration (e.g., slickenside development) overprinting faint horizontal laminations (Fig. 5C). We observed gastropod shells (*Bellamya unicolor*) on slopes throughout Gulfaytu resulting from the erosion of a single 2–5 cm thick limestone-cemented gastropod shell bed located ~20 cm below GT-E (Fig. 5D). Mudstones overlying GT-E vary in thickness due to the erosional base of the overlying carbonate rich pebble conglomerate (Fig. 5E). Beds dip gently to the east ~0–3°, which is consistent with average basin-wide dips of the Hadar Formation measured elsewhere in Ledi-Geraru (Dupont-Nivet et al., 2008).

4.1.2. Busidima-age sediments at Gulfaytu

Above an erosional surface, we mapped a 0.5–1 m thick, clast-supported, moderately sorted conglomerate. It contains sub-rounded pebbles, typically ~1 cm or smaller within a carbonate-rich matrix, though larger pebbles are common (Fig. 5E). The unit forms ledges along the slopes of the Gulfaytu hills and locally displays up to 4 m of erosional relief (Figs. 3 and 5E). The Gulfaytu conglomerate is composed primarily of reworked and rounded pedogenic carbonate nodules (up to 70%), with remaining clasts consisting of dark volcanic pebbles. At some locations, the unit is planar to cross-bedded and we measured dip and dip direction of ~15° and ~112°, respectively on the cross-beds. Fish and crocodile fossils as well as fragments of bivalves and gastropods in the Gulfaytu conglomerate suggest deposition within a perennial fluvial setting. The sediments overlying the Gulfaytu conglomerate are dark brown, bedded to massive sandy mudstones that contain well-sorted, fine gray sandstone layers. These deposits are mapped along hillsides largely covered by gravel lag from erosion of late Quaternary surfaces (see explanation below; Figs. 3 and 4). We did not observe tephras in this section that might be used as chemical or chronological ties to the Busidima Formation. Although this post-conglomerate section is thin (<6 m), its lithology is consistent with descriptions of the Busidima Formation at other lower Awash project areas (e.g., Quade et al., 2004). However, at this time we refrain from attributing these sediments to the Busidima Formation (see discussion section) and refer to them as Busidima-age sediments that unconformably overly the Hadar Formation.

4.1.3. Late Quaternary surfaces

The development of geomorphic surfaces at Gulfaytu follows the late Quaternary history of surface stability and episodic base level lowering of the ephemeral Geraru and Woranso drainages (tributaries to the Awash River; Fig. 2). We distinguished three surfaces based on the degree of pavement development and geomorphic expression (Fig. 3). The highest surface (SIII) is unconformable above Busidima-age sedimentscapping the Gulfaytu hills at ~545 m elevation. It is highly fragmented and eroded with moderate pavement development and varnish coated surface clasts. SII is a prominent surface that gently slopes radially outward from the Gulfaytu hills at elevations ranging from 530 to 540 m. It has moderate pavement development and dark brown varnished surface clasts. Surface I (SI) is inset into SII and is expressed as isolated gravel remnants ~1 m above active channels (O).

4.1.4. Structural geology

Two west-dipping normal faults offset Hadar Formation sediments on the east side of the Gulfaytu hills near the main road (Fig. 3). The southernmost fault strikes 345° and displaces BKT-2U ~6 m against the stratigraphically higher diatomite containing sample LG-184-1 (Fig. 3). Approximately 400 m north, a second fault strikes 310° and displaces BKT-2U ~12 m against Gulfaytu Tuffs B and C. Based on simple displacement-length ratios for normal faults (Kim and Sanderson, 2005), the two faults at Gulfaytu are likely structurally linked and may represent multiple displacement events. Because the Gulfaytu conglomerate is not offset, the faults were likely active prior to the deposition of Busidima-age sediments. This is consistent with post-depositional faulting offsetting the Hadar Formation prior to the deposition of the Busidima Formation elsewhere in the basin (Wynn et al., 2008).

4.2. Tephra descriptions

At Gulfaytu, we mapped (Fig. 3) and described seven new tephra deposits in the Hadar Formation stratigraphically above BKT-2U. Post-BKT-2 tephras range from 1 to 12 cm thick, contain ash to lapilli-sized grains, and show various degrees of alteration including yellow to orange colored scoria clasts, relic pumice grains, and complete alteration to bentonite. We assigned the name 'Gulfaytu Tuffs' followed by a letter (example: GT-X) to denote tephra layers that outcrop at multiple locations. In all other cases we refer to tephras by their sample number. Below, we describe each tephra in stratigraphic order beginning with the oldest.

4.2.1. BKT-2 volcanic complex

The BKT-2 complex at Gulfaytu includes only BKT-2U (sample AM06-1072); BKT-2L is not observed in the section and may be reworked. Two thin basaltic tuffs (samples AM06-1070, and AM06-1069) may be related to the Green Marker Bed (GMB), the lowermost tephra in the BKT-2 complex. The thickest and most complete exposure of BKT-2U is at site LG-185 where it is ~75 cm thick and contains a compositionally and physically distinct clast assemblage including bimodal glass (Table 1) as individual pumice and scoria clasts, abundant feldspar and quartz phenocrysts, and a basal lithic component. We confirmed the presence of BKT-2U at Gulfaytu based on its physical description, glass chemistry (sample AM06-1072; Table 1; Fig. 6), and stratigraphic position within the basin (DiMaggio et al., 2008). Although BKT-2U and -2L have indistinguishable rhyolitic glass chemistry (Campisano and Feibel, 2008b; DiMaggio et al., 2008), we are confident that sample AM06-1072 is BKT-2U and not BKT-2L because the physical appearance and clast assemblage of AM06-1072 is identical to other proximal BKT-2U outcrops in central Ledi-Geraru where BKT-2L is also well-preserved in complete stratigraphic succession (DiMaggio et al., 2008).

4.2.2. Samples LG-227-5 and LG-184-1

At least two distinct bentonites are recognized between BKT-2U

Table 1
Un-normalized major-element geochemistry for glass shards in samples collected at Gulfaytu, Ledu-Geraru research project.

Date run	Location	Sample	Tuff		Compound oxide weight %											
					SiO_2	TiO_2	Al_2O_3	MnO	Fe_2O_3	MgO	CaO	Na_2O	K_2O	Cl	Total	n
06/06/13	site: LG-221	LG-221-4 (mode 1)	Gulfaytu Tuff D	avg	64.80	1.06	12.79	0.12	5.15	0.92	2.87	3.91	2.39		94.01	14
				±1 σ	0.84	0.13	0.13	0.03	0.37	0.14	0.26	0.09	0.10		1.06	
		LG-221-4 (mode 2)		avg	54.13	3.51	13.86	0.18	12.42	4.49	8.35	2.61	1.03		100.59	7
				±1 σ	2.88	0.39	0.15	0.03	1.26	0.84	1.13	0.17	0.29		0.77	
06/06/13	site: LG-718	LG-718-79 (mode 1)	Gulfaytu Tuff D	avg	65.32	1.03	12.70	0.11	5.04	0.85	2.78	3.83	2.40		94.07	7
				±1 σ	0.89	0.11	0.09	0.02	0.38	0.10	0.19	0.15	0.07		1.00	
		LG-718-79 (mode 2)		avg	50.84	4.42	13.67	0.23	14.51	5.05	9.32	2.59	0.78		101.40	7
				±1 σ	1.81	0.47	0.37	0.05	0.83	0.68	1.04	0.18	0.22		0.50	
06/06/13	site: LG-718	LG-718-78	Gulfaytu Tuff C	avg	71.46	0.14	12.91	0.04	1.06	0.17	0.98	3.76	3.21		93.74	15
				±1 σ	0.88	0.03	0.11	0.03	0.05	0.01	0.05	0.24	0.32		1.05	
05/03/10	site: LG-237	LG-237-8	Gulfaytu Tuff C	avg	71.16	0.04	12.67	0.04	1.07	0.10	0.93	3.75	3.30	0.03	93.09	17
				±1 σ	1.70	0.03	0.50	0.03	0.07	0.01	0.14	0.20	0.59	0.04	1.76	
06/25/15	site: LG-207	LG-1000-2	Gulfaytu Tuff C	avg	71.63	0.13	12.87	0.04	1.08	0.09	1.00	3.78	3.50		94.11	20
				±1 σ	0.58	0.08	0.16	0.02	0.05	0.01	0.04	0.18	0.35		0.77	
06/25/15	site: LG-204	LG-1001-2	Gulfaytu Tuff C	avg	71.61	0.15	13.07	0.04	1.05	0.08	0.99	3.96	3.29		94.24	20
				±1 σ	0.90	0.07	0.10	0.02	0.08	0.01	0.04	0.18	0.48		0.97	
06/06/13	site: LG-718	LG-718-77 (mode 1)	Gulfaytu Tuff B	avg	66.61	0.50	12.50	0.13	4.78	0.14	1.59	4.45	2.98		93.69	23
				±1 σ	0.89	0.03	0.10	0.04	0.44	0.02	0.14	0.20	0.08		0.58	
05/03/10	site: LG-204	LG-204-2 (mode 1)	Gulfaytu Tuff B	avg	65.69	0.14	12.44	0.15	5.15	0.09	1.69	4.34	2.99	0.07	92.74	15
				±1 σ	0.87	0.04	0.14	0.04	0.38	0.03	0.13	0.13	0.10	0.03	0.91	
08/28/13	site: LG-204	LG-204-2 (mode 1)	Gulfaytu Tuff B	avg	66.82	0.51	12.54	0.12	4.82	0.08	1.64	4.75	3.16		94.43	13
				±1 σ	0.50	0.11	0.15	0.02	0.33	0.03	0.09	0.18	0.08		0.52	
		LG-204-2 (mode 2)			56.89	2.50	13.68	0.28	12.00	2.32	6.17	3.71	1.71		99.26	1
				±1 σ	–	–	–	–	–	–	–	–	–		–	
08/16/06	site: LG-187	AM06-1075 (mode 1)	Gulfaytu Tuff B	avg	69.52	0.33	12.50	0.14	4.63	0.07	1.60	2.65	2.94		94.38	14
				±1 σ	0.74	0.04	0.10	0.04	0.42	0.06	0.12	0.29	0.14		0.88	
		AM06-1075 (mode 2)		avg	51.63	2.91	13.47	0.24	15.14	4.35	8.68	3.09	0.92		100.42	9
				±1 σ	2.49	0.37	0.17	0.06	1.07	0.73	0.84	0.30	0.26		0.35	
08/28/13	site: LG-187	AM06-1075 (mode 1)	Gulfaytu Tuff B		68.36	0.51	12.06	0.12	4.10	0.07	1.65	4.07	2.86		93.79	1
				±1 σ	–	–	–	–	–	–	–	–	–		–	
		AM06-1075 (mode 2)		avg	49.64	3.90	14.11	0.19	13.74	6.21	10.98	2.64	0.45		101.87	11
				±1 σ	0.45	0.34	0.24	0.04	0.55	0.45	0.51	0.13	0.12		0.86	
01/12/13	site: LG-185	AM06-1072 (mode 1)	BKT-2U	avg	70.54	0.21	11.87	0.06	2.27	0.00	0.48	4.41	3.00		92.84	12
				±1 σ	0.95	0.03	0.18	0.01	0.16	0.00	0.06	1.06	0.15		0.66	
01/12/13	site: LG-185	AM06-1072 (mode 2)	BKT-2U	avg	52.84	3.49	14.44	0.24	14.00	3.84	8.38	3.51	1.11		101.85	5
				±1 σ	0.29	0.14	0.12	0.02	0.18	0.08	0.08	0.15	0.01		0.35	

Notes: See text and Table A.1. for electron microprobe (EMP) running conditions and Table A.2. contains individual glass shard analyses; n is the number of analyses; avg is the average value associated with ±1σ standard deviation. Samples run in 2010 and earlier have inconsistent TiO_2 weight percents.

and GT-A. Sample LG-227-5 is a 4 cm thick bentonite lying ~4–5 m above BKT-2U at site LG-227 (Fig. 4). Feldspar crystals were noted (<1%), but their poor quality (e.g., highly fractured) and low potassium composition made them unsuitable for radiometric dating. The second bentonite (sample LG-184-1, informally referred to as the 'pink tuff') is 2–4 cm thick, contains feldspar phenocrysts, and outcrops in a prominent tan to light pink colored silt ~6 m above BKT-2U (Fig. 3). Although this bentonite layer is discontinuous in outcrop, the encasing silt can be traced along the eastern side of the Gulfaytu hills (Fig. 3).

4.2.3. Gulfaytu Tuffs A through E

GT-A is a 1 cm thick lapilli tephra containing both dark gray unaltered scoria clasts and yellow altered clasts. It is laterally discontinuous and lies 60–100 cm below GT-B (e.g., LG-207; Fig. 4). GT-B is a 5–6 cm thick dark gray ash-fall layer with a sharp basal contact and in places fills desiccation cracks in the underlying clay unit. The deposit is composed of light gray to clear highly stretched (tubular) and frothy pumice, glass shards, and brown scoria clasts. Mafic lithic fragments (~1% or less fraction) were identified at the base of the tephra, but no phenocrysts were observed. GT-C is a ~6–8 cm thick tephra-fall deposit, light gray in color, and is layered with dark and light gray pumice clasts. The tephra is observed outcropping in a light brown silt to mudstone ~30–40 cm above GT-B (though up to 1 m) and ~40 cm below GT-D. Microscope investigations show that GT-C contains white to light gray pumice, <1% dark reddish orange altered scoria clasts and no phenocrysts were observed. GT-D is discontinuous in outcrop and encased in silty mudstone. It is ~4 cm thick, dark gray in color with orange alteration, and fills in desiccation cracks in the underlying mudstone. It is bimodal, containing scoria and elongate pumice clasts, most of which are altered. GT-E is a distinct gray ash layer at some sites and a tuffaceous silt horizon elsewhere. A widespread gastropod-rich limestone bed is present ~20 cm stratigraphically below GT-E. We used the gastropod bed and GT-E as marker beds for lateral correlation of Gulfaytu stratigraphy (Figs. 3, 4 and 5D).

4.3. Electron microprobe glass composition

We used electron microscopy to analyze the major element chemistry of glass shards from Gulfaytu tephras and present the results in Table 1 and in Fig. 6 along with previously published analyses of Busidima and Hadar Formation tephras for comparison. Of the seven post-BKT-2 tephras, one is basaltic (GT-A), one is rhyolitic (GT-C; although it contains <1% altered scoria clasts), two contain bimodal glass (GT-B and GT-D), and three are bentonite layers (including $^{40}Ar/^{39}Ar$ dated sample LG-184-1) that were originally felsic, as indicated by their light color and the frothy morphology of relic pumice. GT-D is the only tephra reported from either the Hadar or Busidima Formation that is dacitic (≤70 wt % SiO_2 and ≤7wt % alkali; normalized), with a second mode ranging from basaltic to basaltic andesite.

Fig. 6 shows variability in the weight percent concentrations of CaO and Fe_2O_3 among tephras from Gulfaytu and other regions in the lower Awash Valley. The only regional correlation supported by these data is BKT-2U at Gulfaytu (sample AM06-1072), which is statistically identical to BKT-2U from Hadar and Ledi-Geraru at a 95% level based on SD analysis ($D < 3.5$) using normalized glass totals (Perkins et al., 1995). Busidima Formation tephras BKT-3 and HE01-168 from Hadar (Campisano and Feibel, 2008b) have similar compositions to Gulfaytu tephras, but can be ruled out as definite correlates due to their age and stratigraphic position (Fig. 6).

4.4. $^{40}Ar/^{39}Ar$ dating of sample LG-184-1

Sixteen single-grain step-heating experiments were performed on feldspars from LG-184-1 (Table 2). The Ca/K ratio of the grains, obtained as a by-product of the argon gas analyses, ranged from ~0.2 to 12 (sanidine to plagioclase), but most fell between 0.5 and 1 (anorthoclase, n = 13).

Incremental release apparent-age spectra for these experiments are shown in Fig. A.1. The majority of grains (14 of 18) yielded an age plateau (defined as a sequence of at least three or more steps representing at least half of the total ^{39}Ar release, and for which analytical error alone is sufficient to explain the observed age dispersion at a probability of 95%). Virtually every plateau encompassed the entire gas release, with one exception, where the plateau encompassed 75% of the total release. With the exception of one imprecise, older outlier grain at 3.8 Ma (plagioclase), the results form a simple symmetric probability distribution, with a weighted-mean age of 2.931 ± 0.017 Ma (1σ) (Fig. 7A).

Inverse–isochron plots for the plateau steps are shown in Fig. A.2, and the distribution of the isochron ages in Fig. 7B. Because almost all the experimental steps yielded high $^{40}Ar^*$ (asterisk denotes radiogenic) content (>90%) and are clustered very close to the X-axis of the inverse isochrons, isotope correlation analysis in this situation is of limited use in defining the 'trapped' $^{40}Ar/^{36}Ar$ component obtained from the intercept of the Y-axis (Table 2). The

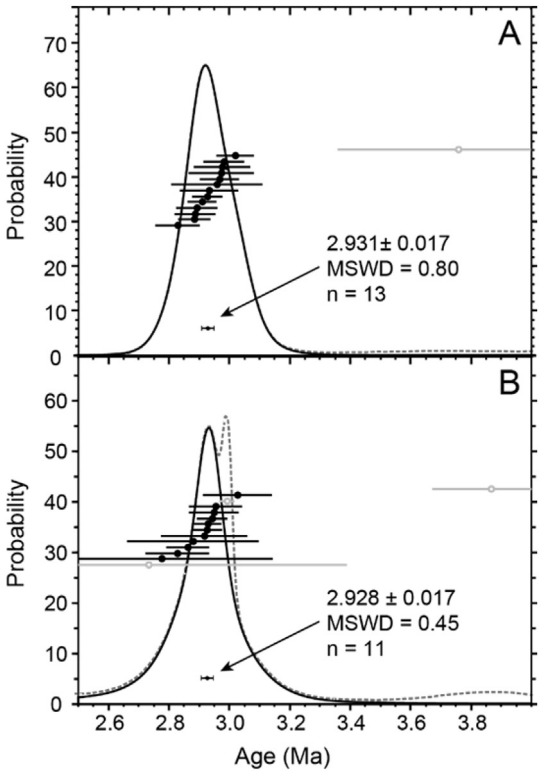

Fig. 7. $^{40}Ar/^{39}Ar$ age-probability spectra of plateau (A), and isochron (B) age experiments of sample LG-184-1. Individual plateau or isochron ages are ordered vertically by age and shown with 1σ analytical uncertainty. Excluded analyses are shown in gray with an open symbol. The solid curved black line is the weighted mean age-probability spectrum, while the gray dashed line includes all analyses (black and gray ages). The weighted mean age of the sample is provided and marked by a diamond shape (1σ error). MSWD is the mean square of the weighted deviation of the included (n = 13 or n = 11) ages. See Appendix A (Tables A.3 and A.4 and Figs. A.1. and A.2.) for a full report of analytical data.

Table 2
Summary of $^{40}Ar/^{39}Ar$ incremental-heating analytical results for sample LG-184-1.

	Apparent age plateau					Integrated age			Inverse isochron age				
Run ID #	Age (Ma ± 1σ)*		MSWD	n/n_{tot}	$\%^{39}Ar$	Age (Ma ± 1σ)			Age (Ma)	± MSE	$(^{40}Ar/^{36}Ar)_{tr}$	± MSE	MSWD
26162-01	2.981	0.08	0.5	5/5	100	3.02	0.13		2.779	0.36	811	1213	0.2
26162-02	2.897	0.06	1.1	4/4	100	2.874	0.061		2.927	0.043	215	49	0.9
26162-03	2.834	0.06	1.3	3/4	81.5	2.816	0.066		2.831	0.15	306	506	2.6
26162-04	2.971	0.06	0.2	4/4	100	2.973	0.068		2.956	0.08	390	202	0.1
26162-05	2.932	0.04	0.6	4/4	100	2.926	0.045		2.946	0.041	238	150	0.9
26162-06	2.887	0.05	0.9	4/4	100	2.885	0.057		2.866	0.066	306	14	1.2
26162-07	2.978	0.1	1.6	4/4	100	2.975	0.088		2.919	0.2	392	451	2.3
26162-08	3.024	0.05	1.0	4/4	100	3.020	0.069		2.994	0.016	64	49	1.1
26162-09	2.96	0.14	1.0	5/5	100	3.05	0.18		2.735	0.66	1459	6489	1.0
26162-10	2.987	0.06	1.2	4/4	100	3.029	0.070		3.029	0.13	519	837	1.6
26162-12	2.913	0.04	0.4	4/4	100	2.914	0.052		2.881	0.21	325	223	0.6
26162-14	2.936	0.09	2.0	4/4	100	2.838	0.080		2.951	0.13	278	152	3.0
26162-15	2.89	0.06	0.9	5/5	100	2.840	0.072		2.931	0.035	151	69	0.8
26162-16	3.76	0.4	1.0	5/5	100	3.74	0.50		3.868	0.19	137	60	0.8
weighted mean	***2.931***	***0.017***						***weighted mean***	***2.968***	***0.012***			
								weighted mean†	***2.928***	***0.019***			

Notes: a solid rectangle encloses aliquots used in calculating weighted means
* includes error in *J* (the neutron fluence parameter)
† weighted mean excluding aliquot 26162-08 (dashed)
MSWD = Mean Square Weighted Deviation
MSE = Modified Standard Error, calculated as the standard error multiplied by root MSWD if the MSWD is greater than one.

isochron age results are also vulnerable to disproportionate influences from single points due to the strong influence of outliers on least-squares minimization procedures. Apart from the one obvious older outlier in Fig. 7B, the weighted mean age of the isochron results is 2.968 ± 0.012 Ma, substantially older than the plateau mean. However, this result appears to be unduly influenced by a single relatively old result (26162-08) with a substantially higher precision than other data values. If this point is considered aberrant (either due to measurement problems, mathematical distortions resulting from the isochron fitting, or is actually a geologically older contaminant) and eliminated, the resulting isochron weighted mean age (2.928 ± 0.019 Ma) is indistinguishable from the plateau mean (Table 2). Given the irregularities evidenced by the isochron result, the plateau weighted-mean result (2.931 ± 0.017 Ma) is taken as the reference age for this sample. This age is for LG-184-1 is consistent with its stratigraphic position ~6 m above the 2.94 Ma BKT-2U.

4.5. Seismic reflection surveys

The seismic reflection data are characterized by shallow reflectivity showing continuous and discontinuous events with variable amplitudes (Fig. 8). Shallow dips (~1°–3°) are evident toward the east or southeast, which is consistent with dips determined from outcrops of Hadar Formation rocks to the west and southwest nearest to the profiles. Local small-scale undulations are also common. On Line 1, a zone of poor reflectivity occurs from the surface ~110 m below which relatively strong, mostly continuous, events extend over the length of the profile (Fig. 8). These deeper events (from ~150 m to ~350 m) may be offset in a few locations by small-scale faults, but precise identification of small faults is difficult due to the poor data quality. Between stations 215 and 270, the events at ~150 m appear to form a low-relief culmination, with events to the east appearing to dip slightly more than those to the west.

Line 2 exhibits similar shallow reflectivity, with gentle apparent dip towards the south-southeast (Fig. 8). Near the northern end of Line 2, seismic events extend to approximately 440 m. This area is crossed by both profiles and similar events to the same apparent depths are not well imaged on Line 1. On both seismic profiles, events below ~350 m are weaker and there are few coherent events that appear to be indicative of real subsurface structure (Fig. 8). As noted previously, loss of reflectivity with increasing depth probably is due to diminished signal penetration from the weight-drop seismic source.

On both profiles, coherent reflectivity begins rather abruptly at a depth of roughly 80–100 m (Fig. 8). Although very near-surface interfaces (<20–30 m) are difficult to clearly image with the receiver and source spacing used in this experiment, the relatively strong first events imaged at ~80–100 m on the profiles were initially thought to correlate with the transition from the vadose zone to water-saturated and relatively more indurated rocks, where the seismic velocity would be expected to increase and below which the rate of signal attenuation would be less. Refraction velocities estimated from first arrivals that reasonably can be associated with reflections in shot records from profiles 1 and 2 are on the order of 2000 m/s and lower. Because these velocities are lower than expected for mafic volcanic flows, we interpreted the reflections to be layering in the lacustrine sediments of the Hadar Formation. However, during the 2014 HSPDP drilling campaign at Gulfaytu and Woranso, located ~1.5 km southwest of the seismic survey (Figs. 2 and 3), drilling demonstrated that the strong reflectors between about ~128 and 213 m (Fig. 8) correlate with basalt layers intercalated with lacustrine mudstones penetrated during drilling (Campisano et al., 2014).

5. Discussion

5.1. New Hadar Formation tephra occurrences

The $^{40}Ar/^{39}Ar$ date of 2.931 ± 0.017 Ma provides a new age constraint for the top of the Hadar Formation. It confirms that the sediments overlying BKT-2U (2.94 Ma) at Gulfaytu are conformable and provide a high resolution record of continued predominantly lacustrine deposition during an important time period. This date and glass geochemistry data offer the possibility for future tephrostratigraphic ties in the region to the post-BKT-2 section at Gulfaytu.

Given the sparse post BKT-2 sedimentological record of the Hadar Formation throughout the lower Awash Valley, it is not surprising that tephra deposits overlying BKT-2U at Gulfaytu do not chemically correlate to other reported tephras (Fig. 6; Roman et al., 2008). The absence of tephras in the 8 m thick post-BKT-2 section at Hadar can be attributed to reworking within Hadar paleosols, erosional processes during deposition, or an eruptive source(s) was proximal to Gulfaytu. DiMaggio et al. (2008) showed paleogeographic variation in BKT-2U tephra thickness and texture, suggesting that BKT-2U was sourced north-northeast of Gulfaytu, possibly from the Ida Ale volcanic center. Ida Ale (Fig. 2) lies only 9 km north of Gulfaytu (~30 km north of Hadar), contains both basaltic and rhyolitic vents and domes reflecting the bimodal nature of Gulfaytu tephras, and was reportedly active between 3.8 Ma – 2.7 Ma (Walter, 1981), coincident with deposition at Gulfaytu. Other possible source regions for the Gulfaytu tephras include the two small domes of Malom Koma adjacent (~1 km) to Gulfaytu (Fig. 2; though the timing of their eruptive phase is unknown), volcanic centers northwest of Ida Ale, or Mt. Ayelu, which has been suggested as a possible source for Busidima Formation tephras (Roman et al., 2008).

Although we have determined the overall stratigraphic order of the tephra deposits at Gulfaytu, not all tephras are laterally continuous (e.g., GT-D). This suggests that the region must have experienced localized erosion during deposition or that tephra dispersal from nearby volcanic domes (Fig. 2) was highly localized. Furthermore, some of the thin tephras (e.g., sample LG-184-1) may have become reworked into encasing sediments and not visible in the outcrop.

A compilation of tephra data by Roman et al. (2008) from the lower Awash Valley highlights important differences between tephras from the Hadar and Busidima Formations based on their relative chronostratigraphic frequency and volcanic glass chemistry. Using the new record of tephras from Gulfaytu, we consider these differences over the new time period expressed by the Gulfaytu strata. First, the observation by Roman et al. (2008) that the relative number of tephras recorded in the lower Awash Valley stratigraphic record is greater in the Busidima Formation than the Hadar Formation is not consistent with the number of new tephras mapped in the Hadar Formation at Gulfaytu (seven post BKT-2 tephras; Fig. 3). Based on the evidence from Gulfaytu, the observed shift in eruption frequency may reflect a shift to a more proximal source region, allowing for more and smaller eruptions to be preserved. The numerous Gulfaytu tephras are also consistent with paleolandscape interpretations that Gulfaytu was within the depocenter of paleolake Hadar during the late Pliocene (DiMaggio et al., 2008), as low energy environments are conducive to tephra preservation (White and Riggs, 2001). Second, Busidima and Hadar Formation tephras tend to differ in the chemistry of their evolved vitric component. In general, Busidima Formation tephras are less evolved (SiO_2 < 75 wt. %) and are often more calcium and iron-rich than Hadar Formation tephras (Roman et al., 2008). Tephras at Gulfaytu show both chemical affinities; glass from BKT-2 and GT-C

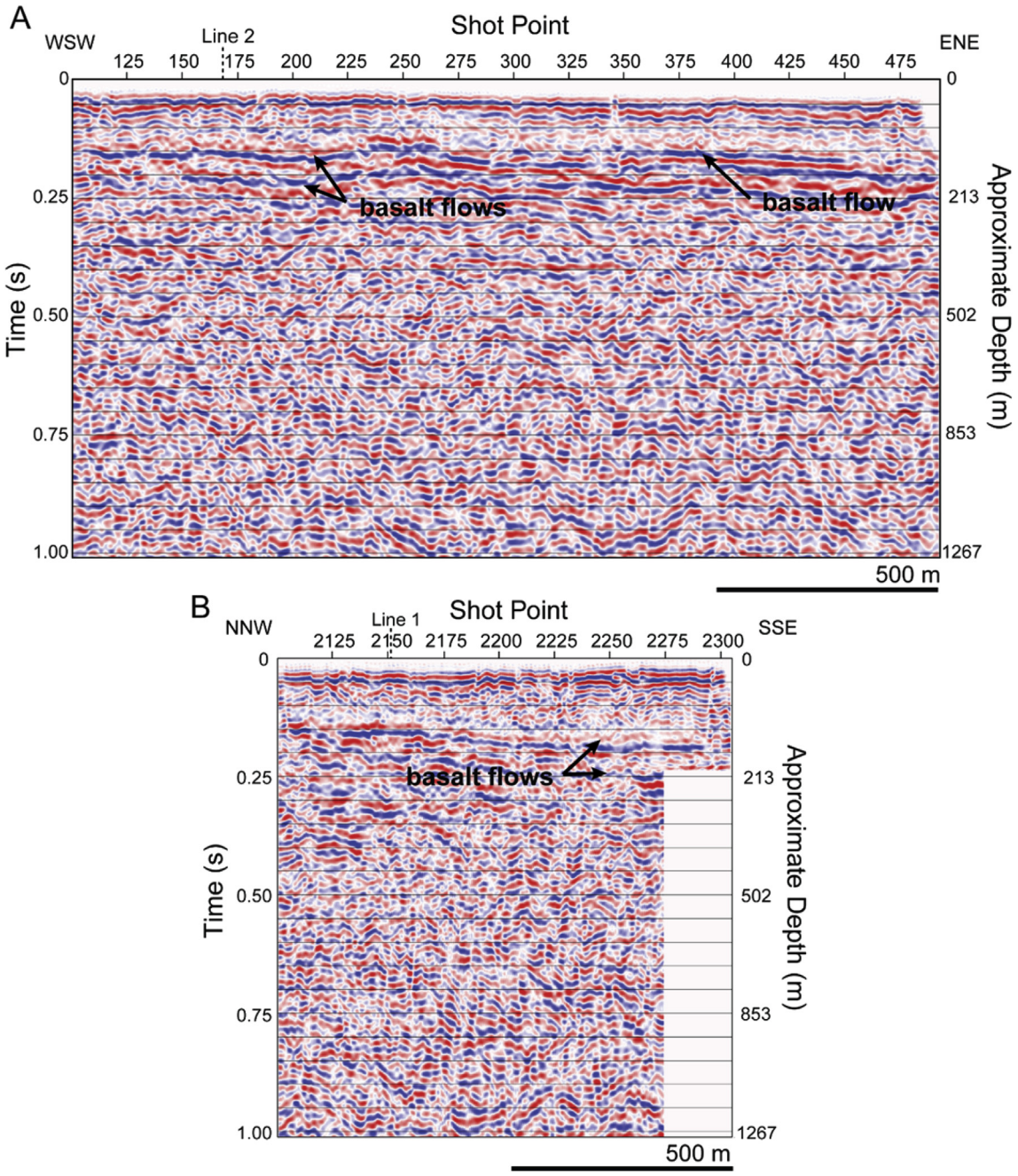

Fig. 8. (A) Line 1. NE-SW (76°) trending seismic reflection profile. Station spacing is 5 m and total line length is 1957 m. Intersection with Line 2 is between stations 164 and 165. (B) Line 2. NW-SE (166°) trending seismic reflection profile. Station spacing is 5 m; total line length is 1017 m. Intersection with Line 1 is at station 2152. For both lines, red represents positive amplitudes and blue represents negative amplitudes, and time section with approximate depths are shown on the right axis. Drilling results indicate that upper reflectors are basalt flows. (For interpretation of the references to colour in this figure legend, the reader is referred to the web version of this article.)

have >75 weight % SiO_2 (normalized), whereas GT-B and GT-D are more similar to the chemical affinities reported for Busidima tephras (<75 weight % SiO_2). Finally, until now, the BKT-2 deposits were the only basaltic or mixed magma tephras reported from the Hadar Formation, though there are interbedded basaltic lava flows including the ~3.30 Ma Kada Damum Basalt (Renne et al., 1993; Tiercelin et al., 1986), the bimodal BRT (~3.78 Ma) from Woranso-Mille (Deino et al., 2010), which is coeval in age with the Hadar Formation, and the slightly older bimodal Cindery Tuff (3.9 Ma) from the middle Awash (Hall et al., 1984). Bimodal eruptions continued after 2.94 Ma and may have become more frequent as indicated by the bimodal compositions observed in tephras from Gulfaytu (e.g., GT-B) and in the Busidima Formation, for example the Salal Me'e Tuff, BKT-3, and AST-1 (Campisano and Feibel, 2008b). Our analysis of Gulfaytu tephras suggests that the timing of the proposed shift in source regions for Hadar and Busidima Formations proposed by Roman et al. (2008) may have commenced during the deposition of the uppermost Hadar Formation possibly reflecting increased activity at the nearby bimodal Ida Ale volcanic center (Walter, 1981) or other proximal sources.

5.2. Paleoenvironmental implications

Although the outcrops of post-BKT-2 deposits are not laterally

extensive across Ledi-Geraru (probably because they are in a topographic culmination of preserved strata), they spatially extend our mapping of the Hadar Formation, providing important controls on interpreting paleoenvironmental and tectono-sedimentary models for the lower Awash Valley. The basalt flows encountered during drilling and recognized post hoc in seismic reflection surveys (Fig. 8; Campisano et al., 2014) underlying Gulfaytu indicate that the predominant lacustrine sedimentation of the Hadar Formation was punctuated by occasional lava emplacement. It is not uncommon in the region to observe basalt flows from the extensive Afar Stratoid Series fissure eruptions interfingering Hadar Formation strata (e.g., Kada Damum). Alternatively, the flows are also proximal to Ida Ale and Malom Koma volcanoes (also active ~3–2 Ma; Walter dissertation) and therefore the Gulfaytu flows may be related to their activity.

We estimate that the newly described Hadar Formation at Gulfaytu represents ~22 kyr of continuous sedimentary and volcanic deposition by applying a deposition rate measured for the Hadar Formation in nearby southern Ledi-Geraru (90 cm/kyr) (Dupont-Nivet et al., 2008) to the similarly lacustrine deposits at Gulfaytu. This estimate is consistent with the minimal age difference (within measurement error of ~30 kyr) between BKT-2U and sample LG-184-1. Thus, lacustrine deposition in the Hadar Basin continued for at least ~22 kyr after the eruption of BKT-2U, until ca. 2.92 Ma.

The established correlation of BKT-2 across much of the Ledi-Geraru area (DiMaggio et al., 2008, Fig. 9) provides a useful stratigraphic constraint for interpreting lateral facies changes. DiMaggio et al. (2008) demonstrated a clear progression in depositional environments near ~2.95 Ma from shallow/fluctuating-lacustrine settings at Hadar to relatively deep lacustrine settings in the central Ledi-Geraru including Gulfaytu. Our work demonstrates that the Hadar Basin remained depositional following the BKT-2 eruptions, and that paleolake Hadar was present at Gulfaytu at this time. Following the eruption of BKT-2U at 2.94 Ma, Lake Hadar regressed, as indicated by laminated clays with evidence of subsequent pedogenesis (Fig. 4). This was followed by transgression ca. 2.93 Ma, when sample LG-184-1 was erupted into the basin. Gulfaytu remained, at least intermittently, a nearshore environment up until the time of the GT-E eruption, as indicated by the laterally extensive gastropod-rich limestone bed spanning Gulfaytu and the presence of weakly developed paleosols. Sometime between ca. 2.92 Ma and 2.7 Ma deposition in the Hadar Basin may have ceased or, if it continued, was subsequently eroded as a direct result of major structural changes affecting basin configuration at this time (Quade et al., 2008; Wynn et al., 2008; Yemane, 1997) and possibly as paleolake Hadar migrated to eastern Ledi-Geraru and the Kariyu Basin, as suggested by Kalb (1995).

In other project areas in the lower Awash, the presence of the BUS and Busidima Formation sediments marks the onset of fluvial and floodplain deposition by the ancestral Awash River system within the N–S trending Busidima half-graben (Quade et al., 2008; Wynn et al., 2008). The relatively thin section (<6 m thick) of post-unconformity sediments at Gulfaytu, primarily sandy mudstones with sand bodies, was likely deposited under similar fluvial conditions. The fossiliferous nature of the pebble conglomerate at Gulfaytu (including crocodile and fish fossils), along with the abundance of pedogenic carbonate nodules, suggests that the oldest conglomerate at Gulfaytu was deposited by perennial stream flow within a larger paleotributary likely to the ancestral Awash River (Fig. 2). However, sediments overlying the erosional unconformity surface at Gulfaytu do not contain diagnostic Busidima Formation strata or tephra deposits, and lie 22 km northeast from the closest documented Busidima Formation outcrop at Hadar (Fig. 9). Therefore, until additional mapping can elucidate the outcrop patterns between Hadar and the Gulfaytu sites, and these sediments are studied in greater detail, we refrain from directly correlating Gulfaytu sediments overlying the erosional unconformity surface to the Busidima Formation. Rather, we refer to the post-unconformity sediments as Busidima-age sediments that unconformably overly the Hadar Formation.

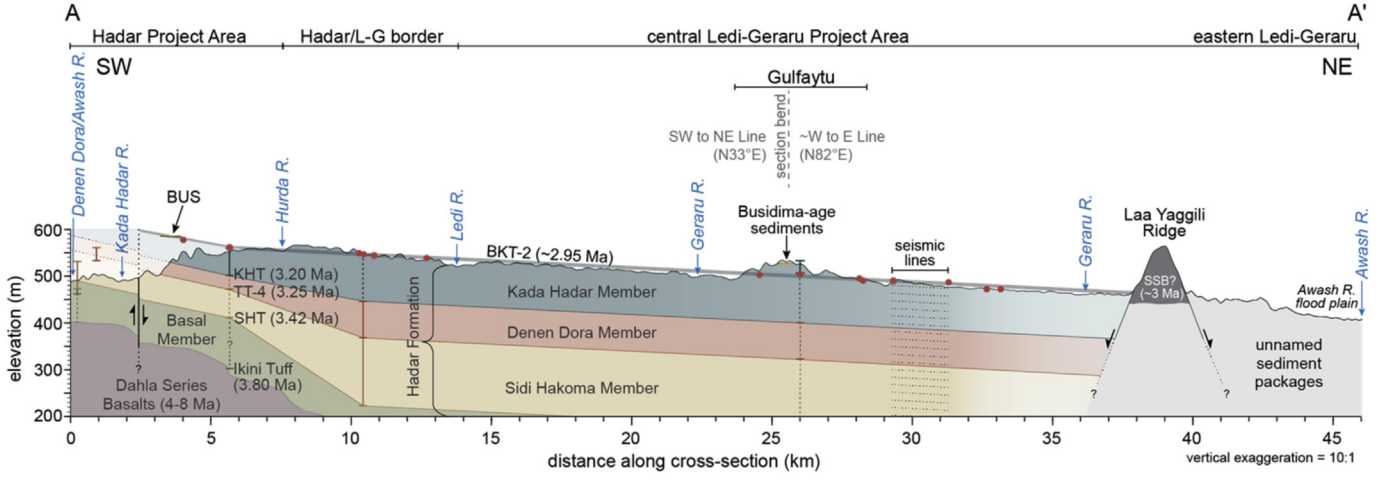

Fig. 9. Interpreted cross-section of the Hadar Basin from the Awash River at Hadar, through Gulfaytu and the Laa Yaggili basalt ridge, ending at the Awash River. See Fig. 1 for profile location. Members of the Hadar Formation are labeled and shaded, and the age of marker bed tephras are provided (see text for age references). The BUS mapped at Hadar (Campisano, 2012) is ~60 m topographically above the unconformity surface mapped at Gulfaytu that marks the base of Busidima-age sediments. The strata exposed at Gulfaytu, and their subsurface continuation are the focus of this paper. Solid vertical lines (color coded by member color) denote published sections (Campisano and Feibel, 2008a,b; Campisano, 2007; Dupont-Nivet et al., 2008; Johanson et al., 1978; Wynn et al., 2008; this study). Dashed vertical lines are approximate and their thicknesses are based on these studies. Dashed section lines below Gulfaytu are equivalent in thickness to section lines at 10.5 km measured in southern Ledi-Geraru (L-G). Although deposition rates at Gulfaytu were likely higher than in southern Ledi-Geraru (see text for discussion), we projected thickness measurements from southern Ledi-Geraru to Gulfaytu to show a *minimum* thickness for the Hadar Formation. Outcrops of BKT-2 are shown as red dots and were projected onto the cross section line from within a 5 km swath (Campisano and Feibel, 2008a,b; DiMaggio et al., 2008; this study). The gray isochron line (2.95 Ma; ~1° dip) connects BKT-2 outcrops from >6 km along the section line, and is consistent with low dip of the Hadar Formation measured in southern Ledi-Geraru (Dupont-Nivet et al., 2008). Black dashed lines denote the location and penetration depth of the seismic survey. SSB = Stratoid Series Basalt.

5.3. Structural implications

We compiled our data along with published regional studies to construct a 40 km long schematic cross-section showing the interpreted geology of the Hadar Basin (Fig. 9). The level of BKT-2 follows a low slope topographic surface (~1° NNE) from the Awash River near Hadar, Gona, and Dikika through central Ledi-Geraru and Gulfaytu east to Laa Yaggili. Incorporating published stratigraphic sections, we demonstrate the slight north and east thickening of the Hadar Formation (Fig. 9). To visualize the thickness of the Hadar Formation below Gulfaytu, we aligned measured sections from southern Ledi-Geraru (referred to as the Middle Ledi in Dupont-Nivet et al., 2008) to the local outcrops of BKT-2 at Gulfaytu. The estimated thickness of the Hadar Formation below Gulfaytu is a minimum estimate because, unlike southern Ledi-Geraru, Gulfaytu was likely positioned within the Hadar Basin depocenter for much of the duration over which the Hadar Formation was deposited and may have experienced higher sedimentation rates. This is demonstrated for at least the Kada Hadar Member by the diatomite encased BKT-2 at most locations near and east of Gulfaytu (DiMaggio et al., 2008).

The Eibdaha fault was suggested as a possible candidate for the border fault controlling the northeast directed deposition of the Hadar Formation (Dupont-Nivet et al., 2008; Quade et al., 2008). While the Eibdiha fault appears to have been active syn-depositional with the Hadar Formation, we do not support it as the Hadar Basin border fault because the northern projection of the fault would intersect with Gulfaytu and be inconsistent with the deposition of Hadar lake sediments at Gulfaytu and additional diatomite-encased BKT-2 deposits in areas ~10 km east (DiMaggio et al., 2008). The west dipping border fault controlling deposition in the Hadar Formation for possibly over a million years (3.8–2.9 Ma) must exist east-northeast of Gulfaytu and all other BKT-2 deposits mapped thus far in Ledi-Geraru as they are in similarly lacustrine units (Fig. 9). A north-northwest striking fault along the Laa Yaggili basalt ridge in eastern Ledi-Geraru (Fig. 9) is a candidate for a Hadar Basin border fault. This fault is east of all known BKT-2 deposits and the accommodation space created along it would afford the north-northeast depositional direction measured at all lower Awash sites. Furthermore, as a major structural weakness, it may have served as a conduit for fissure eruptions during the emplacement of the Laa Yaggili basalt flows, which are mapped as part of the Afar Stratoid Series (Barberi et al., 1975; Kidane et al., 2003), similar to the emplacement of the As Duma basalt along the As Duma fault (Quade et al., 2008). Although we lack additional constraints on the context of the Laa Yaggili fault, including only loosely constrained ages of the basalt flows to the east and north (Barberi et al., 1975; Kidane et al., 2003), and the documentation of any proximal facies deposited against the Laa Yaggili scarp, ongoing work in eastern Ledi-Geraru may provide additional information to elucidate the complex basin configuration in this portion of the lower Awash between 2.9 and 2.7 Ma (DiMaggio, 2013).

The unconformity documented at Gulfaytu, separating the Hadar Formation from Busidima-age sediments, was likely formed due to the same tectonic reorganization of basin architecture in the region as that which defines the base of the Busidima half-graben. First, the stratigraphic position of the erosional surface at Gulfaytu is consistent with, though 20 m above, the first major erosional surface truncating the Hadar Formation elsewhere in the basin (Wynn et al., 2008). We also observe a change in facies above the unconformity surface to sandy mudstones with interbedded sand bodies. Second, whereas descriptions of conglomerate beds immediately overlying the BUS are variable among lower Awash project areas, the basal conglomerate at Gulfaytu is consistent with descriptions of the KH-5 conglomerate at Hadar, a ~3 m thick pebble conglomerate with abundant reworked carbonate nodules, and the G2 unit at Gona, a clast-supported planar to cross-stratified pebble conglomerate (Campisano, 2012; Quade et al., 2004) suggesting a similar origin. Third, we rule out the possibility that the Gulfaytu conglomerate is a young geomorphic feature based on field observations that show significant differences between the expression of the unsorted, pebble to cobble late Quaternary surface deposits and the cross-bedded carbonate nodule-rich conglomerate at Gulfaytu. Lastly, the As Duma Fault controlled the formation of the Busidima half-graben that led to the deposition of the Busidima Formation. The fault is mapped for ~23 km striking ~ N–S along the western slope break of the western escarpment (Fig. 6E in Campisano, 2012, Fig. 1 in Quade et al., 2008). If central Ledi-Geraru was not located within the Busidima half-graben (i.e., post-unconformity Gulfaytu sediments were not deposited in the Busidima half graben), based on the above observations (unconformity, facies change) the Gulfaytu region was at least affected by the regional tectonic changes to basin architecture.

Nevertheless, we leave open the possibility that the erosional surface mapped at Gulfaytu (Fig. 3) is the northeastern continuation of the Busidima unconformity surface (BUS) mapped throughout Hadar, Gona, and Dikika (Campisano, 2012; Quade et al., 2008; Wynn et al., 2008). This would imply that post-unconformity sediment deposition at Gulfaytu is contiguous with and related to the 'wedge' of fluvial sediments and tephras deposited in the Busidima half-graben.

6. Conclusions

The Gulfaytu area in central Ledi-Geraru preserves the youngest documented strata of the Hadar Formation. We add 20 m of previously undescribed sediments, including 7 new tephras, to the Kada Hadar Member of the Hadar Formation. An altered tephra dated to 2.931 ± 0.017 Ma constrains the top of the Hadar Formation, which is consistent with the position of Gulfaytu strata conformably above BKT-2U. Based on sedimentation rates, the top of the Hadar Formation is ~2.92 Ma in central Ledi-Geraru. The chemical fingerprints of interbedded tephras offer the possibility for tephrostratigraphic ties from the newly defined Kada Hadar sediments to other areas, including critical outcrop-to-core correlations for the Afar HSPDP chronostratigraphic framework (Campisano et al., 2014). Gulfaytu deposits are dominantly lacustrine in origin, indicating that the paleolake within the greater Hadar Basin depocenter persisted after 2.94 Ma as did the configuration of the Hadar Basin. The subsurface geology adjacent to Gulfaytu is characterized by thick gently dipping beds that are relatively unaffected by large offset faults, which supports previous work placing the Hadar Basin depocenter in the general area of central Ledi-Geraru. Lava flows encountered by the HSPDP are interbedded with the lacustrine units. The presence of an unconformity surface truncating the Hadar Formation and the package of overlying sediments suggests that central Ledi-Geraru was affected by the changes to regional basin architecture after 2.92 Ma. This study shows that the Gulfaytu region was not as deeply eroded after 2.94 Ma, as other regions of the lower Awash Valley, which sets the stage for continued investigation of outcrops elsewhere in the lower Awash that may further reveal basin dynamics and depositional environments between 2.9 Ma and 2.7 Ma, a time period also critical for paleoanthropology investigations.

Acknowledgments

We would like to thank the Authority for Research and Conservation of Cultural Heritage (A.R.C.C.H.) and the Ministry of

Culture and Tourism of Ethiopia for permitting our research endeavors. For logistical and field support we are grateful to our Addis field crew, our A.R.C.C.H. representative Solomon Kebede, our kind Afar friends from the Mille area, and the Institute of Human Origins. We thank Gordon Moore as well as the personnel in the LeRoy Eyring Center for Solid State Science at ASU for their laboratory assistance and Dominique Garello for her help preparing and analyzing samples. This manuscript was greatly improved by comments from Kay Behrensmeyer, an anonymous reviewer, and the editor. This project was funded in part by the Leakey Foundation, the Wenner Gren Foundation for Anthropological Research, the Institute of Human Origins and School of Human Evolution and Social Change at Arizona State University and by NSF grant EAR-0725553. This is contribution #4 of the Hominin Sites and Paleolakes Drilling Project.

Appendix A. Supplementary data

Supplementary data related to this article can be found at http://dx.doi.org/10.1016/j.jafrearsci.2015.09.018.

References

Alemseged, Z., Spoor, F., Kimbel, W.H., Bobe, R., Geraads, D., Reed, D., Wynn, J.G., 2006. A juvenile early hominin skeleton from Dikika, Ethiopia. Nature 443, 296–301.

Arrowsmith, J.R., Reed, K.E., Lockwood, C.A., Jones, K., 2004. Geological mapping and tephrostratigraphy of the Hadar Formation near 11.25 N and 40.75 E (Afar Region, Ethiopia). Geol. Soc. Am. Abstr. Progr.s 36, 487.

Audin, L., Quidelleur, X., Coulie, E., Courtillot, V., Gilder, S., Manighetti, I., Gillot, P.Y., Tapponnier, P., Kidane, T., 2004. Palaeomagnetism and K-Ar and Ar-40/Ar-39 ages in the Ali Sabieh area (Republic of Djibouti and Ethiopia): constraints on the mechanism of Aden ridge propagation into southeastern Afar during the last 10 Myr. Geophys. J. Int. 158, 327–345.

Barberi, F., Ferrara, G., Santacroce, R., Varet, J., 1975. Structural evolution of the Afar triple junction. In: Schweizer, E. (Ed.), Verlagsbuchhandl. Naegele u. Obermiller, Stuttgart.

Behrensmeyer, A.K., 2008. Paleoenvironmental context of the Pliocene A.L. 333 "First Family" hominin locality, Hadar Formation, Ethiopia. Geol. Soc. Am. Spec. Pap. 446, 203–214.

Best, M.G., Christiansen, E.H., Deino, A.L., Gromme, C.S., Anonymous, 1995. The Central Nevada Caldera Complex in the Middle Tertiary Ash-flow Province of the Great Basin, USA. International Union of Geodesy and Geophysics. General Assembly 21, Week A, 444.

Campisano, C., Feibel, C., 2008a. Depositional environments and stratigraphic summary of the Pliocene Hadar Formation at Hadar, Afar depression, Ethiopia. Geol. Soc. Am. Spec. Pap. 446, 179–201.

Campisano, C., Feibel, C., 2008b. Tephrostratigraphy of the Hadar and Busidima Formations at Hadar, Afar depression, Ethiopia. Geol. Soc. Am. Spec. Pap. 446, 135–162.

Campisano, C.J., 2007. Tephrostratigraphy and Hominin Paleoenvironments of the Hadar Formation, Afar Depression, Ethiopia. Rutgers The State University of New Jersey - New Brunswick, United States – New Jersey.

Campisano, C.J., 2012. Geological summary of the Busidima Formation (Plio-Pleistocene) at the Hadar paleoanthropological site, Afar depression, Ethiopia. J. Hum. Evol. 62, 338–352.

Campisano, C.J., Cohen, A., Asrat, A., Feibel, C., Kingston, J., Lamb, H., Olago, D., Owen, R., Renaut, R., Schabitz, F., 2014. The Hominin Sites and Paleolakes Drilling Project (HSPDP) drilling campaigns: the trials and triumphs of trying the unique and new. In: 2014 GSA Annual Meeting in Vancouver, British Columbia.

Campisano, C.J., Feibel, C.S., 2007. Connecting local environmental sequences to global climate patterns: evidence from the hominin-bearing Hadar Formation, Ethiopia. J. Hum. Evol. 53, 515–527.

Cohen, A., Arrowsmith, R., Behrensmeyer, A.K., Campisano, C., Feibel, C., Fisseha, S., Johnson, R., Bedaso, Z.K., Lockwood, C., Mbua, E., Olago, D., Potts, R., Reed, K., Renaut, R., Tiercelin, J.-J., Umer, M., 2009. Understanding paleoclimate and human evolution through the Hominin Sites and Paleolakes Drilling Project. Sci. Drill. 8, 60–65.

Cohen, A., Umer, M., 2009. Connecting scientific drilling and human evolution. Eos Trans. AGU 90, 122.

Deino, A.L., Scott, G.R., Saylor, B., Alene, M., Angelini, J.D., Haile-Selassie, Y., 2010. 40Ar/39Ar dating, paleomagnetism, and tephrochemistry of Pliocene strata of the hominid-bearing Woranso-Mille area, west-central Afar Rift, Ethiopia. J. Hum. Evol. 58, 111–126.

deMenocal, P.B., 1995. Plio-Pleistocene African Climate. Science 270, 53–59.

deMenocal, P.B., 2004. African climate change and faunal evolution during the Pliocene-Pleistocene. Earth Planet. Sci. Lett. 220, 3–24.

DiMaggio, E., 2013. The Geologic History of Central and Eastern Ledi-Geraru, Afar, Ethiopia. School of Earth and Space Exploration. Arizona State University, p. 573.

DiMaggio, E.N., Campisano, C.J., Arrowsmith, J.R., Reed, K.E., Swisher, C.C., Lockwood, C.A., 2008. Correlation and stratigraphy of the BKT-2 volcanic complex in west-central Afar, Ethiopia. Geol. Soc. Am. Spec. Pap. 446, 163–177.

DiMaggio, E.N., Campisano, C.J., Rowan, J., Dupont-Nivet, G., Deino, A.L., Bibi, F., Lewis, M.E., Souron, A., Garello, D., Werdelin, L., Reed, K.E., Arrowsmith, J.R., 2015. Late Pliocene fossiliferous sedimentary record and the environmental context of early Homo from Afar, Ethiopia. Science 347, 1355–1359.

Dupont-Nivet, G., Sier, M., Campisano, C.J., Arrowsmith, J.R., DiMaggio, E., Reed, K., Lockwood, C., Franke, C., Husing, S., 2008. Magnetostratigraphy of the eastern Hadar Basin (Ledi-Geraru research area, Ethiopia) and implications for hominin paleoenvironments. Geol. Soc. Am. Spec. Pap. 446, 67–85.

Froggatt, P.C., 1992. Standardization of the chemical analysis of tephra deposits; report of the ICCT Working Group. Quat. Int. 13–14, 93–96.

Gibbons, A., 2013. How a Fickle climate made us human. Science 341, 474–479.

Haile-Selassie, Y., Saylor, B.Z., Deino, A., Alene, M., Latimer, B.M., 2010. New hominid fossils from Woranso-Mille (Central Afar, Ethiopia) and taxonomy of early Australopithecus. Am. J. Phys. Anthro. 141, 406–417.

Hall, C.M., Walter, R.C., Westgate, J.A., York, D., 1984. Geochemistry, Stratigraphy, and Geochemistry of Cindery Tuff in Pliocene Hominid-Bearing Sediments of the middle Awash, Ethiopia. Nature 308, 26–31.

Hayward, N.J., Ebinger, C.J., 1996. Variations in the along-axis segmentation of the Afar Rift system. Tectonics 15, 244–257.

Hunt, J.B., Hill, P.G., 1993. Tephra geochemistry; a discussion of some persistent analytical problems. Holocene 3, 271–278.

Johanson, D.C., Taieb, M., 1976. Plio-Pleistocene hominid discoveries in Hadar, Ethiopia. Nature 260, 293–297.

Johanson, D.C., Taieb, M., Coppens, Y., 1982. Pliocene Hominids from the Hadar Formation, Ethiopia (1973–1977) – stratigraphic, chronologic, and paleoenvironmental contexts, with notes on hominid morphology and systematics. Am. J. Phys. Anthro. 57, 373–402.

Johanson, D.C., Taieb, M., Gray, B.T., Coppens, Y., 1978. Geological Framework of the Pliocene Hadar Formation (Afar, Ethiopia) with Notes on Paleontology Including Hominids, vol. 6. Geological Society, London, Special Publications, pp. 549–564.

Kalb, J.E., 1995. Fossil elephantoids, Awash paleolake basins, and the Afar triple junction, Ethiopia. Palaeogeogr. Palaeoclimatol. Palaeoecol. 114, 357–368.

Kerrick, D.M., Eminhizer, L.B., Villaume, J.F., 1973. The role of carbon film thickness in electron microprobe analysis. Am. Mineralogist 58, 920–925.

Kidane, T., Courtillot, V., Manighetti, I., Audin, L., Lahitte, P., Quidelleur, X., Gillot, P.Y., Gallet, Y., Carlut, J., Haile, T., 2003. New paleomagnetic and geochronologic results from Ethiopian Afar: block rotations linked to rift overlap and propagation and determination of a similar to 2 Ma reference pole for stable Africa. J. Geophys. Res. 108.

Kim, Y.-S., Sanderson, D.J., 2005. The relationship between displacement and length of faults; a review. Earth Sci. Rev. 68, 317–334.

Kimbel, W.H., 1996. Hominid Speciation and Pliocene Climatic Change. Yale University Press, New Haven, CT.

Kimbel, W.H., Delezene, L.K., 2009. "Lucy" redux: a review of research on *Australopithecus afarensis*. Am. J. Phys. Anthropol. 140, 2–48.

Kimbel, W.H., Johanson, D.C., Rak, Y., 1994. The first skull and other new discoveries of Australopithecus afarensis at Hadar, Ethiopia. Nat. Lond. 368, 449–451.

Kimbel, W.H., Walter, R.C., Johanson, D.C., Reed, K.E., Aronson, J.L., Assefa, Z., Marean, C.W., Eck, G.G., Robe, R., Hovers, E., Rak, Y., Vondra, C., Yemane, T., York, D., Chen, Y., Evensen, N.M., Smith, P.E., 1996. Late Pliocene Homo and Oldowan tools from the Hadar Formation (Kada Hadar member), Ethiopia. J. Hum. Evol. 31, 549–561.

Kuiper, K.F., Deino, A., Hilgen, F.J., Krijgsman, W., Renne, P.R., Wijbrans, J.R., 2008. Synchronizing rock clocks of Earth history. Science 320, 500–504.

Lahitte, P., Gillot, P.-Y., Kidane, T., Courtillot, V., Bekele, A., 2003. New age constraints on the timing of volcanism in central Afar, in the presence of propagating rifts. J. Geophys. Res. 108, 2123.

Lee, J.Y., Marti, K., Severinghaus, J.P., Kawamura, K., Yoo, H.S., Lee, J.B., Kim, J.S., 2006. A redetermination of the isotopic abundances of atmospheric Ar. Geochim. Cosmochim. Acta 70, 4507–4512.

Perkins, M.E., Nash, W.P., Brown, F.H., Fleck, R.J., 1995. Fallout tuffs of Trapper Creek, Idaho – A record of Miocene explosive volcanism in the Snake River Plain volcanic province. Geol. Soc. Am. Bull. 107, 1484–1506.

Quade, J., Levin, N., Semaw, S., Stout, D., Renne, R., Rogers, M., Simpson, S., 2004. Paleoenvironments of the earliest stone toolmakers, Gona, Ethiopia. Geol. Soc. Am. Bull. 116, 1529–1544.

Quade, J., Levin, N.E., Simpson, S.W., Butler, R., McIntosh, W.C., Semaw, S., Kleinsasser, L., Dupont-Nivet, G., Renne, P., Dunbar, N., 2008. The geology of Gona, Afar, Ethiopia. Geol. Soc. Am. Spec. Pap. 446, 1–31.

Reed, K.E., 2008. Paleoecological patterns at the Hadar hominin site, Afar Regional State, Ethiopia. J. Hum. Evol. 54, 743–768.

Renne, P., Walter, R., Verosub, K., Sweitzer, M., Aronson, J., 1993. New data from Hadar (Ethiopia) support orbitally tuned time scale to 3.3 Ma. Geophys. Res. Lett. 20, 1067–1070.

Renne, P.R., Swisher, C.C., Deino, A.L., Karner, D.B., Owens, T.L., DePaolo, D.J., 1998. Intercalibration of standards, absolute ages and uncertainties in 40Ar/39Ar dating. Chem. Geol. 145, 117–152.

Roman, D.C., Campisano, C., Quade, J., DiMaggio, E., Arrowsmith, J.R., Feibel, C., 2008. Composite tephrostratigraphy of the Dikika, Gona, Hadar, and Ledi-Geraru

project areas, northern Awash, Ethiopia. Geol. Soc. Am. Spec. Pap. 446, 119–134.
Semaw, S., Renne, P., Harris, J.W.K., Feibel, C.S., Bernor, R.L., Fesseha, N., Mowbray, K., 1997. 2.5-million-year-old stone tools from Gona, Ethiopia. Nature 385, 333–336.
Semaw, S., Rogers, M.J., Quade, J., Renne, P.R., Butler, R.F., Dominguez-Rodrigo, M., Stout, D., Hart, W.S., Pickering, T., Simpson, S.W., 2003. 2.6-million-year-old stone tools and associated bones from OGS-6 and OGS-7, Gona, Afar, Ethiopia. J. Hum. Evol. 45, 169–177.
Semaw, S., Simpson, S.W., Quade, J., Renne, P.R., Butler, R.F., McIntosh, W.C., Levin, N., Dominguez-Rodrigo, M., Rogers, M.J., 2005. Early Pliocene hominids from Gona, Ethiopia. Nat. Lond. 433, 301–305.
Simpson, S.W., Quade, J., Levin, N.E., Butler, R., Dupont-Nivet, G., Everett, M., Semaw, S., 2008. A female homo erectus Pelvis from Gona, Ethiopia. Science 322, 1089–1092.
Taieb, M., Johanson, D.C., Coppens, Y., Aronson, J.L., 1976. Geological and paleontological background of Hadar hominid site, Afar, Ethiopia. Nature 260, 289–293.
Tesfaye, S., Harding, D.J., Kusky, T.M., 2003. Early continental breakup boundary and migration of the Afar triple junction, Ethiopia. Geol. Soc. Am. Bull. 115, 1053–1067.
Tiercelin, J., Frostick, L., Renaut, R., Reid, I., 1986. The Pliocene Hadar Formation; Afar Depression of Ethiopia.
Trauth, M.H., Maslin, M.A., Deino, A.L., Strecker, M.R., Bergner, A.G.N., Duhnforth, M., 2007. High- and low-latitude forcing of Plio-Pleistocene East African climate and human evolution. J. Hum. Evol. 53, 475–486.
Villmoare, B., Kimbel, W.H., Seyoum, C., Campisano, C.J., DiMaggio, E.N., Rowan, J., Braun, D.R., Arrowsmith, J.R., Reed, K.E., 2015. Early Homo at 2.8 Ma from Ledi-Geraru, Afar, Ethiopia. Science 347, 1352–1355.
Walter, R.C., 1981. The Volcanic History of the Hadar Early-man Site and the Surrounding Afar Region of Ethiopia, p. 426.
Walter, R.C., 1994. Age of Lucy and the 1st Family - single-crystal AR-40/AR-39 dating of the Denen Dora and Lower Kada Hadar members of the Hadar Formation, Ethiopia. Geology 22, 6–10.
Walter, R.C., Aronson, J.L., 1993. Age and source of the Sidi Hakoma Tuff, Hadar Formation, Ethiopia. J. Hum. Evol. 25, 229–240.
White, J.D.L., Riggs, N.R., 2001. Introduction; styles and significance of lacustrine volcaniclastic sedimentation. Special Publ. Int. Assoc. Sedimentol. 30, 1–6.
White, T.D., Asfaw, B., Beyene, Y., Haile-Selassie, Y., Lovejoy, C.O., Suwa, G., WoldeGabriel, G., 2009. Ardipithecus ramidus and the Paleobiology of Early Hominids. Science 326, 75–86.
White, T.D., Asfaw, B., DeGusta, D., Gilbert, H., Richards, G.D., Suwa, G., Howell, F.C., 2003. Pleistocene Homo sapiens from middle Awash, Ethiopia. Nat. Lond. 423, 742–747.
White, T.D., WoldeGabriel, G., Asfaw, B., Ambrose, S., Beyene, Y., Bernor, R.L., Boisserie, J.-R., Currie, B., Gilbert, H., Haile-Selassie, Y., Hart, W.K., Hlusko, L.J., Howell, F.C., Kono, R.T., Lehmann, T., Louchart, A., Lovejoy, C.O., Renne, P.R., Saegusa, H., Vrba, E.S., Wesselman, H., Suwa, G., 2006. Asa Issie, Aramis and the origin of Autralopithecus. Nat. Lond. 440, 883–889.
WoldeGabriel, G., Heiken, G., White, T.D., Asfaw, B., Hart, W.K., Renne, P.R., 2000. Volcanism, tectonism, sedimentation, and the paleoanthropological record in the Ethiopian rift system. Geol. Soc. Am. Spec. Pap. 345, 83–99. Volcanic Hazards and Human Antiquity.
Wolfenden, E., Ebinger, C., Yirgu, G., Deino, A., Ayalew, D., 2004. Evolution of the northern main Ethiopian rift: birth of a triple junction. Earth Planet. Sci. Lett. 224, 213–228.
Wynn, J.G., Alemseged, Z., Bobe, R., Geraads, D., Reed, D., Roman, D.C., 2006. Geological and palaeontological context of a Pliocene juvenile hominin at Dikika, Ethiopia. Nature 443, 332–336.
Wynn, J.G., Roman, D.C., Alemseged, Z., Reed, D., Geraads, D., Munro, S., 2008. Stratigraphy, depositional environments, and basin structure of the Hadar and Busidima Formations at Dikika, Ethiopia. Geol. Soc. Am. Spec. Pap. 446, 87–118.
Yemane, T., 1997. Stratigraphy and Sedimentology of the Hadar Formation, Afar, Ethiopia. Iowa State University, Ann Arbor, p. 182.
Yilmaz, O., 2001. Seismic Data Analysis: Processing, Inversion, and Interpretation of Seismic Data. Society for Exploration Geophysics, Tulsa, OK.